Design of 2.7 μm Wavelength Er³⁺ Doped ZBLAN Lasers Based on Simulations and Experimental Evidence

Cameron Berge



Department of Electrical & Computer Engineering McGill University Montréal, Québec, Canada

May 2017

A thesis submitted to McGill University in partial fulfillment of the requirements of the degree of Master of Engineering

© Copyright 2017 All rights reserved

Abstract

This thesis presents research made on 2.7 μ m wavelength emitting erbium doped ZBLAN lasers as a source of mid-infrared light. Specifically, the goal of this research is to closely study the erbium energy level mechanisms that give rise to gain at 2.7 μ m, in order to model and design an efficient compact laser source with low power requirements. To achieve these goals, a fluorescent source is built to compare resulting spectra at low power with the pumping wavelengths of 980 nm and 790 nm, as well as provide experimental basis for modeling. Subsequently, a free space pumped laser design is tested, however due to the ZBLAN fiber design leading to high losses, the lasing threshold could not be reached. Consequently, a new fiber design is proposed and tested through a computational model of the erbium doped ZBLAN laser.

Abrégé

Cette thèse présente des recherches effectuées sur les lasers ZBLAN dopés à l'erbium à $2.7~\mu\mathrm{m}$ comme source de lumière infrarouge moyenne. Plus précisément, l'objectif de cette recherche est d'étudier de près les mécanismes du niveau d'énergie de l'erbium qui donnent lieu à un gain à $2.7~\mu\mathrm{m}$, afin de modéliser et de concevoir une source laser compacte efficace avec de faibles besoins en énergie. Pour atteindre ces objectifs, une source fluorescente est construite pour comparer les spectres résultants à faible puissance avec les longueurs d'onde de pompage de 980 nm et 790 nm, ainsi que fournir une base expérimentale pour la modélisation. Par la suite, nous testons une conception laser pompée en espace libre, mais en raison de la conception de la fibre ZBLAN conduisant à des pertes élevées, nous n'avons pu atteindre le seuil d'émission laser. Par conséquent, une nouvelle conception de fibre est proposée et testée à l'aide d'un modèle de calcul du laser ZBLAN dopé à l'erbium.

Acknowledgements

I would like to thank my supervisor Martin Rochette for being a constant positive presence throughout my master's degree, he always provided good advice and direction. I would also like thank Alaa Al-Kadry for helping me in the early stages of my project and teaching me how to succeed in experimental work. Thanks to professor Lawrence Chen for allowing me to use his equipment. Finally, thanks to McGill University for making me feel at home throughout my master's degree.

Contents

1	Intr	oducti	ion	1
	1.1	Applic	cations	1
		1.1.1	Medical	2
		1.1.2	Communications	3
		1.1.3	Manufacturing and Controls	3
		1.1.4	Environmental Monitoring	3
	1.2	Curre	nt State of Research	4
	1.3	Thesis	S Outline	5
2	Bas	ic Con	acepts	6
	2.1	Fiber	Mode and Free-Space theory	6
		2.1.1	ZBLAN Fiber Basics	6
		2.1.2	Fiber Mode Theory	7
		2.1.3	Mode Coupling	8
		2.1.4	Gaussian Beams	10
	2.2	Laser	and Amplifier Theory	11
		2.2.1	Emission and Absorption Basics	11
		2.2.2	Rare Earth Dopants	13
		2.2.3	Spontaneous Emission	14
		2.2.4	Stimulated Emission and Absorption	15

Contents

		2.2.5	Basic Laser Principle and types	16
		2.2.6	Laser levels	18
		2.2.7	Physics of Er^{3+} ZBLAN	19
		2.2.8	Pumping at a Wavelength of 980 nm	19
		2.2.9	Pumping at a Wavelength of 790 nm	21
3	Flu	orescei	nce Measurements	24
	3.1	Fluore	escence Experiment	25
		3.1.1	Fluorescence Source Design	25
		3.1.2	Coupling Efficiency Discussion	26
		3.1.3	Fluorescence Results	27
	3.2	Er^{3+} 2	ZBLAN Free-Space Pumped Laser	33
		3.2.1	Linear Free-Space Pumped Set-up	34
		3.2.2	Loss Analysis	34
		3.2.3	Forward and Backward Pumped Laser	36
		3.2.4	Fiber Issues	37
		3.2.5	Suggestions and Conclusions	39
4	Mo	deling		41
	4.1	Simula	ation Description and Assumptions	41
	4.2	Simula	ation Results	45
		4.2.1	Pumping a 2000 ppm Er:ZBLAN Fiber With A 790 nm Wave-	
			length	46
		4.2.2	Pumping a 2000 ppm Er:ZBLAN Fiber With a 980 nm Wave-	
			length	48
		4.2.3	Predicted Performance of a 70000 PPM Fiber	51
	4.3	Summ	ary of Results	54

57

References

List of Tables

3.1	The measured output signal power at a wavelength of 1310 nm used	
	to determine the mode coupling efficiency experimentally	26
3.2	Summary of the launched and inserted pump powers for the fluores-	
	cence spectrum experiment. Measurements made by using power meter	
	detailed in Figure 3.1	28
3.3	Summary of the total fluorescence measured and power at 2.7 μm for	
	the fluorescence experiment. Measurements made by using power me-	
	ter detailed in Figure 3.1 using a long pass filter for isolated 2.7 $\mu\mathrm{m}$	
	power	29
3.4	Loss in the free-space portion of the laser cavity	34
3.5	Suggested ZBLAN fiber characteristics	39
3.6	Mode characteristics at each wavelength of interest. *values for LP01	
	mode only	40
3.7	Mode characteristics at each wavelength of interest. *values for LP01	
	mode only	40

List of Figures

1.1	Atmospheric window transmission showing which chemicals are respon-	
	sible for absorption. [1]	2
1.2	Graphic showing different mid-infrared reactive chemicals and their	
	corresponding wavelength and application $[4]$	4
1.3	Graphic showing different mid-infrared reactive chemicals relevant to	
	the field of medicine. [3] \dots	4
2.1	Crossection of optical fiber showing the core and clad regions with n_1	
	and n_2 refractive indices respectively	7
2.2	First 3 modes in circular step index waveguide. A: 1st mode (LP01)	
	B: 2nd mode (LP11) C: 3rd mode (LP21)	8
2.3	Showing a single mode fiber transmitting its mode into fiber which has	
	a different single mode shape. [11]	9
2.4	Beam divergence of three different initial beam waists	11
2.5	The waist size difference of three different lenses	11
2.6	Left: classic model of an electron in orbit around a nucleus releasing	
	light from transitioning from an energetic outer shell E2 to the ground	
	state shell E1. Right: The same electron transition represented in a	
	bandgap diagram format.	12

List of Figures v

Energy diagram of rare earth ions. The red dots indicate the energy	
states that are expected to emit in UV, Visible, or Infrared part of the	
optical spectrum [14]	14
Basic diagram of a circular ring cavity laser where ϵ is the through port	
coupling coefficient	17
Basic diagram of a linear cavity laser where R1 and R2 are input and	
output mirrors respectively	17
System diagram of how a laser operates. G, L and R represent signal	
gain, loss and reflection coefficient respectively	17
Different kinds of laser schemes, with colors representing the popula-	
tion at that level (red is high population density, blue is low population	
density)	19
Important energy level diagram showing transitions with 980 nm pump-	
ing [2]	20
980 nm pumping energy levels showing how ETU process increases	
efficiency. [2]	20
Energy level diagram with relevant processes when pumping with a	
wavelength of 790 nm. [2]	22
Measured Erbium absorption crossections from around the wavelength	
of 790 nm. Note the order of magnitude difference between absorption	
from the upper laser level ${}^4\mathrm{I}_{11/2}$ compared to the ESA from the lower	
laser level ${}^4I_{13/2}$ [2]	22
The experimental set-up of an Er^{3+} - ZBLAN fiber fluorescent source.	25
The loss spectrum of the erbium doped ZBLAN fiber provided by the	
manufacturer Fiber Labs. Note the window showing losses between	
1000 nm and 1550 nm	27
	optical spectrum [14]. Basic diagram of a circular ring cavity laser where ϵ is the through port coupling coefficient. Basic diagram of a linear cavity laser where R1 and R2 are input and output mirrors respectively. System diagram of how a laser operates. G, L and R represent signal gain, loss and reflection coefficient respectively. Different kinds of laser schemes, with colors representing the population at that level (red is high population density, blue is low population density). Important energy level diagram showing transitions with 980 nm pumping [2]

List of Figures vi

3.3	An example of direct coupling between two fibers depicting the differ-	
	ence between launched and inserted power. Notice within the small	
	alignment error dx there is some loss of light	28
3.4	Linear scale spectral results of the fluorescence experiment using a 980	
	nm pump signal	28
3.5	Linear scale spectral results of the fluorescence experiment using a 790	
	nm pump signal	28
3.6	the fluorescence experiment, left hand side shows the pump direct cou-	
	pled to the input of a 5m $\mathrm{Er^{3+}}$ ZBLAN fiber	30
3.7	Energy level diagram showing the relevant energy transitions for 980	
	nm and 790 nm pumping, color coded for suspected population levels.	
	Energy levels and transitions are based on [2] [17]	31
3.8	Output Spectrum for varying 790 nm pump powers superimposed with	
	the 980 nm pump output spectrum. Green: 75 mW, Blue: 85 mW,	
	Cyan: 35 mW, Black: 100 mW of 980 nm. Note: powers listed are	
	inserted powers A. Residual Pump. B: 2.7 μm signal	32
3.9	Linear free-space coupled laser cavity	34
3.10	Comparison of output fluorescence while using direct coupling (orange)	
	and free-space coupling (blue). the grey line depicts a threshold fluo-	
	roescence value where 2.7 μm could be first detected	35
3.11	Example of best achieved free space coupling given all the losses	36
3.12	Much more powerful direct coupling is giving an intense green glow .	36
3.13	New design with forward and backward pumping to resolve the loss issue	36
3.14	Diagram of a fiber showing the yaw (β) and pitch (α) axis used for	
	angular alignment	38
4.1	Showing the fiber cut into N subsections with the red gradient repre-	
	senting the pump absorption	42

List of Figures vii

4.2	Energy level diagram the 790 nm pump simulations are based on [17].	42
4.3	Energy level diagram the 980 nm pump simulations are based on [12].	42
4.4	The experimental/simulated 790 nm wavelength absorption through	
	25 cm of 2000 ppm fiber (black/blue)	46
4.5	Simulated spectrum using 790 nm wavelength with the 2000 ppm fiber.	46
4.6	$2700~\mathrm{nm}$ signal power and $790~\mathrm{nm}$ pump power as a function of distance.	46
4.7	Population densities of important population levels at the beginning	
	middle and end of the fiber for a 2000 PPM Er:ZBLAN fiber pumped	
	at a wavelength of 790 nm	48
4.8	Simulated spectrum using 980 nm wavelength with the 2000 ppm fiber.	49
4.9	$2700~\mathrm{nm}$ signal power and $980~\mathrm{nm}$ pump power as a function of distance.	49
4.10	Population densities of important population levels at the beginning	
	middle and end of the fiber for a 2000 PPM Er:ZBLAN fiber pumped	
	at a wavelength of 980 nm	50
4.11	790 nm wavelength pumping. Notice how the weak free-space coupled	
	$790~\mathrm{nm}$ signal remains strong enough to fluoresce at $550~\mathrm{nm}$ at the end	
	of a 3 m length fiber.	50
4.12	980 nm wavelength pumping. Notice how the strong direct-coupled	
	980 nm signal is no longer strong enough to fluoresce after about 1.5	
	m traveled in the fiber	50
4.13	Simulated spectrum using 790 nm wavelength with the 70000 ppm fiber.	51
4.14	$2700~\mathrm{nm}$ signal power and $790~\mathrm{nm}$ pump power as a function of distance.	51
4.15	Population densities of important population levels at the beginning	
	middle and end of the fiber for a 70000 PPM Er:ZBLAN fiber pumped	
	at a wavelength of 790 nm	52
4.16	Simulated spectrum using 980 nm wavelength with the 70000 ppm fiber.	53
4.17	2700 nm signal power and 980 nm pump power as a function of distance.	53

List of Figures viii

	8 Population densities of important population levels at the beginning
	middle and end of the fiber for a 70000 PPM Er:ZBLAN fiber pumped
54	at a wavelength of 980 nm

List of Terms

ETU : Energy transfer upconversion

GSA: Ground state absorption

ESA: Excited state absorption

GSB: Ground state bleaching

CR: Cross relaxation

ull: Upper laser level

lll: Lower laser level

ZBLAN: Glass composed of $ZrF_4 - BaF_2 - LaF_3 - AlF_3 - NaF$

 Er^{3+} : Erbium ion

SMF-28: Single mode optical fiber made of silica glass

ASE: Amplified spontaneous emission

Chapter 1

Introduction

In this thesis, we report the results of a research dedicated to the fabrication of a fiber laser source at the mid-infrared wavelength of 2.7 μ m through the use of erbium doped ZBLAN fibers. Specifically, by delving into the physics behind erbium ion interactions when embedded in ZBLAN glass, we seek to know the viability of low power, compact, and efficient coherent fiber sources of mid-infrared wavelengths. Such mid-infrared coherent light sources, which emit at wavelengths between 2 and 20 μ m of the electromagnetic spectrum, find uses in various application fields ranging from communications to medical, and chemical process controls in manufacturing to environmentally conscious pollution detectors, many of which rely on atomic interactions at such mid-infrared wavelengths.

1.1 Applications

The most widespread applications of $\mathrm{Er^{3+}}$ doped ZBLAN fiber lasers are detailed in this section. Figure 1.1 shows the transmission of Earth's atmospheric window with respect to wavelength.

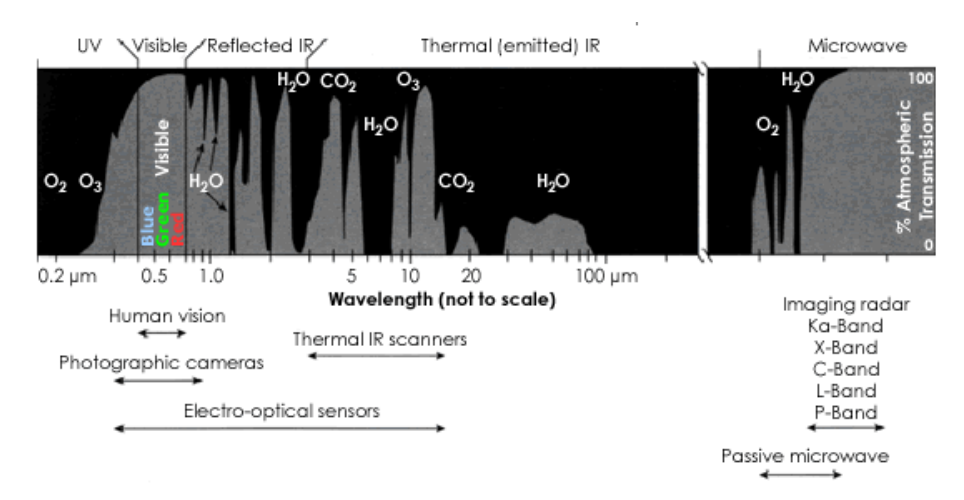


Fig. 1.1 Atmospheric window transmission showing which chemicals are responsible for absorption. [1]

1.1.1 Medical

A 2.7 μ m laser source has numerous applications in the field of medicine. A direct application of such sources is in laser scalpels for surgery [2]. Because water is highly absorbing at $\sim 3 \mu$ m, as observed in figure 1.1, water molecules in skin tissue react to this light by inducing a clean, aseptic surgical cut. Using lasers over metal scalpels is advantageous because spot size can be controlled for incision accuracy, and bacteria is not transferred through light. Multiple other applications in medicine are based on using spectrum sensing for diagnosis or health monitoring [3]. Figure 1.3 shows many of the organic compounds that have absorption resonances in the mid-infrared region of light. These compounds can be detected and quantified by concentration levels based on absorption measurements. Nonlinear optical processes are used to broaden the spectrum of a mid-infrared light source to target different compounds. One such application is a glucose meter for diabetics that requires an optical source of $\sim 9 \mu$ m [4]. In order to attain this wavelength from a 3 μ m laser, a third order nonlinear processes such as three-wave mixing can be used [5].

1.1.2 Communications

As seen in figure 1.1, there is a high transmission band in the atmosphere between 2.5-2.7 μ m. A coherent source within those wavelengths is useful for airplane and satellite communication [4].

1.1.3 Manufacturing and Controls

Using the 2.7 μ m wavelength source in combination with nonlinear effects, in ways similar to what was discussed for medicine, broadband light can be used to measure concentrations of process chemicals under test. Companies could make use of this by making accurate measurements of chemical concentrations in their manufacturing processes to ensure quality yields and safety [4]. Figure 1.2 shows some of the common process gases and their corresponding absorption wavelengths, for instance Carbon Tetrafluoromethane CF_4 and Ammonia NH_3 .

1.1.4 Environmental Monitoring

With the onset of global warming and significant environmental concerns, it is practical to have sensors which can monitor pollution levels in real-time. One such application of mid infrared light is to detect car tailpipe emissions to collect data on pollution [4]. Since hydrocarbons absorb in the 3-4 μ m range, as shown in figure 1.2. Other applications include monitoring pollutants near precious resources such as fresh water lakes and be able to detect environmental changes in real-time, reducing response time for preventative reaction.

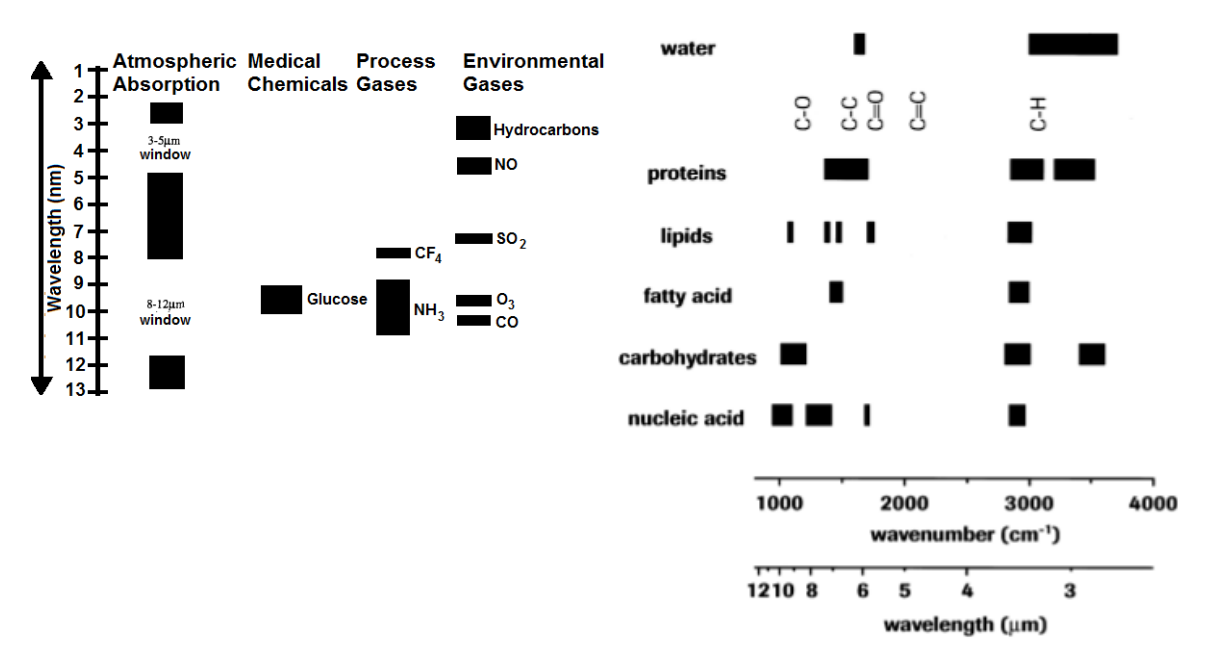


Fig. 1.2 Graphic showing different mid-infrared reactive chemicals and their corresponding wavelength and application [4]

Fig. 1.3 Graphic showing different mid-infrared reactive chemicals relevant to the field of medicine. [3]

1.2 Current State of Research

Research making use of erbium's 2.7 μ m wavelength transition to access the midinfrared began with erbium doped crystals. In these systems, the output power was limited due to a poor heat management and thermooptical properties of the crystal, leading to overheating and breaking [2]. A currently active research area involving the use of Er^{3+} for the generation of mid-infrared light is one of fiber-based sources [2]. Most research being done in this area centers around achieving maximum output powers using fluoride glass based fibers such as ZBLAN. For instance, Er:ZBLANfibers are pumped by as much as 100 W and 75 W, to achieve output powers of up to 10 W and 12 W at a wavelength of 3 μ m [6] [7]. Another approach enables laser wavelengths as long as 3.5 μ m by using two pumping wavelengths: 980 nm and 1973 nm for high order excited state absorptions which achieve lasing between highly energetic states [8]. This presented work differs on the current state of research

by seeking to minimize size of the laser source as an additional constraint to pump conversion efficiency and output power. However, this research is only a first step towards the direction of compact efficient sources in a field dominated by maximizing output power with additional consideration for pump efficiency.

1.3 Thesis Outline

The outline of this thesis is structured as follows: in chapter two, the required laser and optical fiber theory are explained. Subsequently, in chapter three, the results and significance of two main experiments carried out in the masters duration are presented. The first being a fluorescent source which yields promising results, in which strong fluorescence is observed at 2.7 μ m and reported in [9]. The second, a free-space coupled laser source which is determined non-viable due to losses and efficiency issues. As a result of the identified infeasibility, a solution to the problem is recommended, namely a new Er³⁺ doped ZBLAN fiber which has characteristics to correct problems with the initial one. Next, in chapter four the laser is modeled and simulations are made to validate the new fiber design and predict the performance. Finally conclusions are drawn based on a combination of experimental and simulation evidence, and the new fiber design is deemed beneficial.

Chapter 2

Basic Concepts

2.1 Fiber Mode and Free-Space theory

Certain elements of optical fiber theory are required in order to understand how a fiber laser operates. Namely, how light propagates within the fiber, how it couples from one fiber to another, and how it propagates in free space. For example, how light is distributed in a doped fiber affects how it interacts with the dopant in the core. Doping, optical modes and their subsequent interactions will be further expanded on in this chapter. Moreover, coupling between two fibers, via free-space propagation or direct physical connections, can be source of loss, and therefore pertinent to the discourse on laser design. Laser fundamentals will be explained later, for now a brief review of pertinent optical fiber theory is given.

2.1.1 ZBLAN Fiber Basics

ZBLAN is a fluoride based glass which is an acronym for $ZrFM_4 - BaF_2 - LaF_3 - AlF_3 - NaF$. Fibers made from ZBLAN exhibit low loss transmission between the optical wavelength range of 0.250 μ m and 5 μ m and have low phonon energies of $\sim 500-600~\rm cm^{-1}$. These characteristics are advantageous over common silicate based fibers which are lossy above 2 μ m, and have high phonon energies of 1,100 cm⁻¹

which is known to favor non-radiative decay when used in gain media such as lasers or amplifiers [10].

2.1.2 Fiber Mode Theory

When light travels in a medium of high refractive index surrounded by one of lower index such as water and air, there is a critical angle $\theta_C = sin^{-1}(\frac{n_2}{n_1})$, $n_2 < n_1$ [11] after which all of the light is internally reflected. This phenomenon is called total internal reflection. Consider now an optical fiber as shown in figure 2.1, where n_1 is the core material made of slightly higher refractive index as n_2 which is in the cladding area.

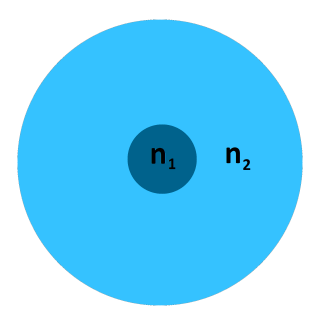


Fig. 2.1 Crossection of optical fiber showing the core and clad regions with n_1 and n_2 refractive indices respectively.

After studying the electric field components of light propagating down a fiber, it was discovered that light can only propagate in certain allowed configurations called modes. Modes of light are essentially the power of standing waves of the electric field and come as solutions to a Bessel differential equation [11]. Since Bessel functions are periodic, there exist many possible mode configurations. The first three mode types are shown in figure 2.2. The most important mode is the first mode called the LP01 (linearly polarized 01) which has a 96% overlap with a gaussian distribution, and as such is well approximated by [11]

$$E(r) = E_0 e^{-\left(\frac{r}{w_0}\right)^2} \tag{2.1}$$

where w_0 is the mode field radius, a point where the mode intensity falls to 1/e of its maximum value. r is the distance from the center of a fiber. E_0 is the electric field strength at r = 0.

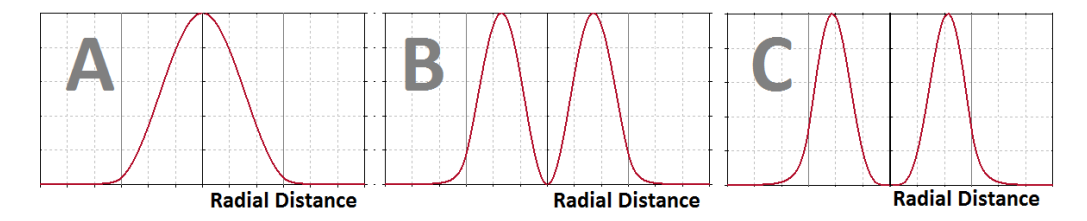


Fig. 2.2 First 3 modes in circular step index waveguide. A: 1st mode (LP01) B: 2nd mode (LP11) C: 3rd mode (LP21)

In order to get an idea of how many modes are in a fiber, there exists a parameter called normalized frequency V. V = $k_0 r_{core} NA$, where $k_0 = \frac{2\pi}{\lambda}$, r_{core} is the fiber core radius, and NA = $\sqrt{n_1^2 - n_2^2}$. NA is known as the acceptance angle. For an optical fiber to be operating in the single mode regime, the V number must be below 2.405. Since everything except for k_0 depends wholly on the fiber characteristics, there always exists a cut-off wavelength below which there is a danger of exciting higher order modes, thus the cut-off wavelength is $\lambda_{cutoff} = \frac{2\pi}{2.405} NA$ [11]. A useful approximation to find the first order mode radius w_0 , if V and the core radius are known [12]

$$w_0 = r_{core}(0.65 + 1.619V^{-1.5} + 2.879V^{-4})$$
(2.2)

2.1.3 Mode Coupling

When working with standardized fibers such as SMF-28 and attempting to send light into a specially designed doped fiber for a laser, it is rare that both fibers will have perfectly matched modes. This is even the case if both fibers operate in single mode. Non-perfect mode matching leads to coupling losses. For example, when a mode is being transmitted from one fiber to a non-matching fiber, as shown in figure 2.3, the

total amount of power transferred is an overlap integral between the two mode shapes as shown in equation 2.3

$$\eta = \left[\frac{4\beta_i \beta_t}{(\beta_i + \beta_t)^2}\right] \frac{\left[\int E_t(r,\phi) E_i^*(r,\phi) dr d\phi\right]^2}{\int E_t(r,\phi) E_t^*(r,\phi) r dr d\phi \int E_i(r,\phi) E_i^*(r,\phi) r dr d\phi}$$
(2.3)

where $E_t(r,\phi)$ and $E_i(r,\phi)$ are the electric field distributions, and β_i , β_t are the

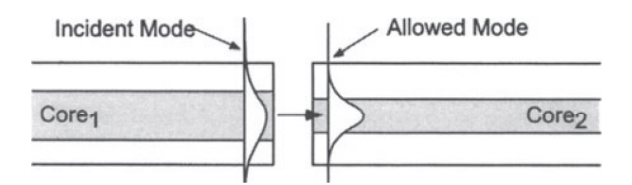


Fig. 2.3 Showing a single mode fiber transmitting its mode into fiber which has a different single mode shape. [11]

propagation constants of the transmitted and incident modes respectively. Thus, if a single mode fiber is matched to a multimode fiber, the incident LP01 mode will be decomposed into a linear combination of possible modes in the multimode fiber. However, if we only consider the efficiency of transmission of the LP01 mode of both fibers, equation 2.3 can be put into the following form [11]

$$\eta = \frac{4w_1^2 w_2^2}{(w_1^2 + w_2^2)^2} \tag{2.4}$$

where w_1, w_2 are the mode radii of the incident and transmitting fibers. If it is required to maximize the coupling between two different LP01 modes, it is possible to transform one of them to match the other through the use of lenses. This leads to the discussion on gaussian beams in the next section.

When light travels through an interface of two transmitting materials of different refractive indices n_1 and n_2 , the refractive index mismatch causes a partial reflection of light. This type of reflection is called a Fresnel reflection. The following equation describes Fresnel reflections in the case where light is incident on an interface Γ_F $\left(\frac{n_1-n_2}{n_1+n_2}\right)^2$. When optical fibers terminate in free-space, the mode of light experiences a new refractive index of 1, different from that of the glass core which is close to 1.5 for silica or ZBLAN glass leading to Fresnel reflection of $\left(\frac{1.5-1}{1+1.5}\right)^2 = \left(\frac{0.5}{2.5}\right)^2 \approx 0.04$ [11], the approximation is due to an uncertainty on the wavelength variation of the refractive index of the glass. Thus a back reflection occurs. Some fibers are cleaved (cleanly cut) at an angle such that the Fresnel reflected light is outside of the fiber's acceptance angle to stop back reflection. The erbium doped ZBLAN is cleaved flat hence exhibits Fresnel reflections at both ends of the fiber. As will be discussed in section 2.2, reflections are beneficial in laser design because they introduce positive feedback.

2.1.4 Gaussian Beams

Since the LP01 mode matches so closely with a spacial Gaussian distribution, the propagation in free space of such beams are important to understand. The fundamental equations for gaussian beams are listed below

$$w(z) = w_0 \sqrt{1 + (\frac{z}{z_R})^2}$$
 (2.5)

$$R(z) = z[1 + (\frac{z_R}{z})^2]$$
 (2.6)

$$z_R = \frac{\pi n w_0^2}{\lambda_0} \tag{2.7}$$

where w_0 is the initial beam waist, z is distance traveled, and z_R is the Rayleigh range, defined as the distance that the beam must propagate to get to $\sqrt{2}$ times its initial size. Since z_R is proportional to the square of the initial beam waist size, the divergence of the Gaussian beam is heavily dependent on w_0 as shown in figure 2.4. In order to make a Gaussian beam couple into a fiber efficiently, the beam radius at the input of the receiving fiber must match as closely as possible to the LP01 mode it expected. In these cases, the following formula for spot size is useful [10]

$$d_{spot} = 4F_{lens}M^2 \frac{\lambda}{\pi * D} \tag{2.8}$$

D is the laser beam diameter at the lens before focusing, M^2 is the beam quality parameter, which is usually close to 1 for Gaussian beams, F_{lens} is the focal point of the lens in use. It can be concluded that minimizing the focal length decreases the lower limit on spot size [10]. Figure 2.5 shows how the focal length of a lens changes the resulting minimum waist size. Thus, when coupling into a doped fiber for the purpose of making a laser, equation 2.8 can be used to match the modes for optimum efficiency.

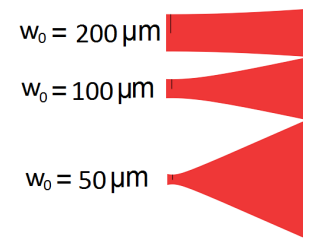


Fig. 2.4 Beam divergence of three different initial beam waists.

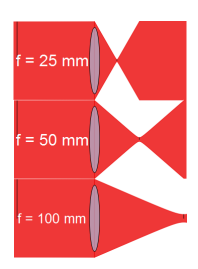


Fig. 2.5 The waist size difference of three different lenses.

2.2 Laser and Amplifier Theory

In this section we go over the basic laser theory framework within which the experimental and simulation components are based.

2.2.1 Emission and Absorption Basics

A first important concept of laser theory are the different ways light can be absorbed and emitted from an atom. In quantum theory, it was realized that electrons configure themselves around atomic nuclei in discrete energy bands. Figure 2.6 represents the classical view of an orbiting electron transiting from one orbit to a lower one, releasing

a photon. The released photon in figure 2.6 has an equal energy as the difference between the two levels: $hf = \Delta E = E_2 - E_1$, where h is Plancks constant, and f is the frequency of the resulting light. In a similar fashion, if light is incident on

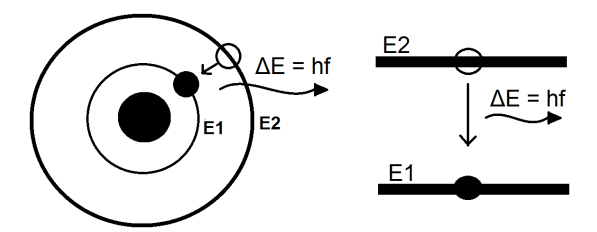


Fig. 2.6 Left: classic model of an electron in orbit around a nucleus releasing light from transitioning from an energetic outer shell E2 to the ground state shell E1. Right: The same electron transition represented in a bandgap diagram format.

an atom, there is a chance that the atom will absorb the light and an electron will transition from a lower energy level E_1 to a higher energy level E_2 where $E_1 + hf = E_2$. If $E_1 + hf$ is not equal to a possible excitation state of the electron, no absorption will occur. In the absence of any excitation other than heat, the energy levels of an atom are configured according to a Boltzmann distribution [13]

$$\frac{N_n}{N_m} = \frac{\rho_n}{\rho_m} e^{\frac{E_m - E_n}{k_B T}} \tag{2.9}$$

where $N_{n,m}$ are the energy level $\rho_{m,n}$ are the statistical weight of each state n,m respectively, n<m. k_B is the Boltzmann constant, and T is temperature in units of Kelvin. Thus at room temperature, very few electrons are in excited states, and almost all are in the lowest energy state called the ground state [13]. There are three types of emission and absorptions possible: Spontaneous emission, and stimulated emission and absorption.

2.2.2 Rare Earth Dopants

Ions of Rare earth metals such as erbium, thulium and ytterbium are commonly used as dopants in optical fibers due to their special spectroscopic properties. Doping is a technique of depositing ions of such metals into the atomic structure of a host glass or crystal. As light in an optical fiber is guided through the core, it interacts with the embedded ions by exciting electrons to higher energy levels by way of stimulated absorption. Following an initial excitation of electrons from the lowest energy level, known as ground state absorption abbreviated GSA, there results a interplay between the three photon-electron interactions: stimulated emission, stimulated absorption, and spontaneous emission. Excited electrons can be further excited by a process known as excited state absorption or ESA, or they can emit photons or phonons (vibrations in the host material equivalent to heat dissipation) and spontaneously relax down to a lower energy state. A further possibility, which is essential to the mechanics of lasers, some photons can cause electrons to transition from a more energetic state to a lesser leading to the generation of photons with same direction, wavelength, polarization, and phase also known as coherent to one another. Each rare earth ion has its own unique electron level configurations that lead to different spectroscopic identities. The energy levels for different ions are shown in figure 2.7.

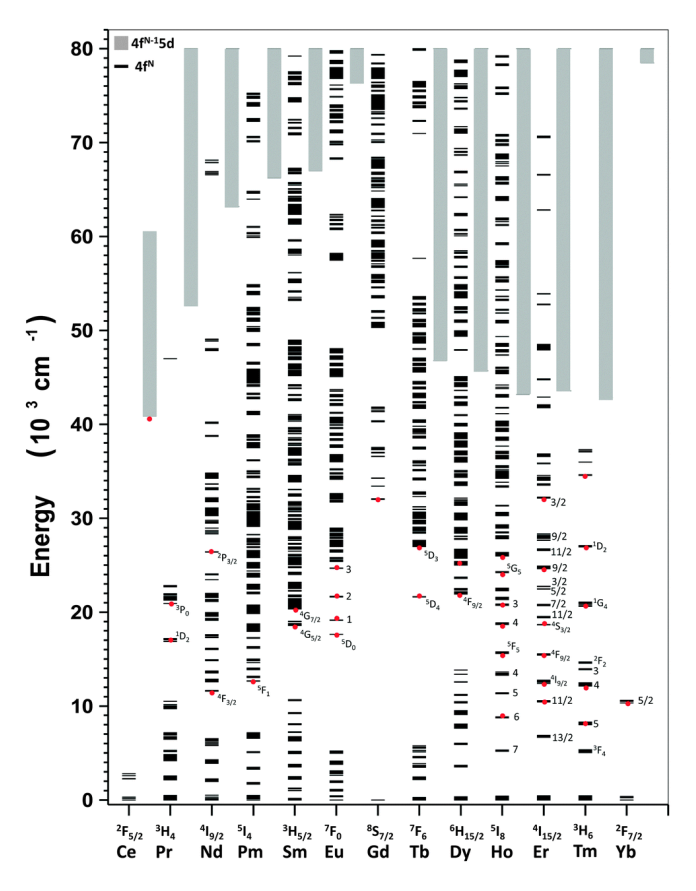


Fig. 2.7 Energy diagram of rare earth ions. The red dots indicate the energy states that are expected to emit in UV, Visible, or Infrared part of the optical spectrum [14].

A standard convention for labeling each energy level is as follows: ${}^{2S+1}L_J$ where in the upper left term (2S+1) is known as the multiplicity with S and integer representing quantum spin. L and J denote the total angular and orbital angular momentum respectively with J being an integer or half integer. L is given a letter (S,P,D,F,...) that represents a whole number (1,2,3,4,...) [11].

2.2.3 Spontaneous Emission

Every energy level in an atom, with the exception of ground state has limited lifetime. The time it takes for an electron to decay is related to its specific intrinsic lifetime τ , which is the time it takes for an excited electrons to decay to e^{-1} of their initial

value, as represented in the following equation [13]

$$N_i(t) = N_i(t=0)e^{-t/\tau_i} (2.10)$$

where τ_i is the intrinsic lifetime of the ith energy level, t is time, and N_i is the population density of energy level i. Not all decaying electrons radiate light, some energy is dissipated as heat or vibrations in the material lattice, otherwise known as phonons. If an excited state is populated, decaying electrons are split between lower energy levels by a factor called a branching ratio [15] denoted by β . The term β does not specify whether or not an electron transition resulted in radiative emission or heat dissipation, but only what fraction of decayed electrons ended at each lesser energetic level. In order to quantify the radiative fraction of spontaeuously transitioning electrons the term γ_{ij} is used where i > j and i, j are energy levels.

2.2.4 Stimulated Emission and Absorption

Stimulated emission occurs when incoming light inspires an electron to transition down between two energy levels N_2 to N_1 and release light of the same frequency and phase [13]. Stimulated absorption is when an atom is forced to absorb incoming light because it has the correct energy to excite an electron, this is the same concept discussed in the previous section. In this part the equations for both of these processes will be discussed.

The equation for the number of pump and Signal photons available for stimulated absorption and emission R_{ij} , R_{SE} respectively, with units of $Photons/m^3$. Where i, j denote energy levels, i < j. [12]:

$$R_{ij} = \frac{\lambda_p \Gamma_p \sigma_{ij}}{hc A_{eff}} N_i P_P \tag{2.11}$$

$$R_{SE} = \frac{\lambda_S \Gamma_S \sigma_{se}}{hc A_{eff}} [N_2 - N_1] P_S$$
 (2.12)

Where $\lambda_{P/S}$ is the pump/signal wavelength, $\Gamma_{P/S}$ is the pump/signal power filling factor, $\sigma_{ij/SE}$ is the cross-section of stimulated Absorption/Emission, N_i is the population density of energy level i, $P_{P/S}$ is the pump/signal power, A_{eff} is the effective area of the pump/signal mode, h is Planck's constant, and c is the speed of light. The light filling factor Γ represents how much of the doped core is being used by the optical mode. There are two general rules: if the propagating light is a single mode, the filling factor is calculated with: $1 - e^{-2(\frac{r_{core}}{w_0})^2}$ [12]. If the light is propagating in multimode it can be assumed that the superposition of each mode completely overlaps the active core, in which case the power filling factor Γ is the ratio of the fibers doped active area to the pump core area. This ratio is always 1, unless the pump is sent in a double clad fiber, in which it would be approximately $\Gamma_P = \pi r_{core}^2/\pi r_{doubleclad}^2$.

The most important concept to note about equations 2.12 and 2.11 is that the amount of absorption depends only on material and fiber constants except for the population of the absorbing level, and the population difference between two levels in the case of stimulated emission. Thus it is of utmost importance to maintain population inversion between the two responsible for generating the laser signal.

2.2.5 Basic Laser Principle and types

This subsection briefly describes the core concept of what optically pumped lasers are, how they can be implemented, and explains the basic mechanics of how they function. Figures 2.8 and 2.9 show two common types of laser cavities, circular and linear. The circular cavity is pumped through a wavelength division multiplexer and allowed to circulate through a gain medium which produces a laser signal that is sent to an output by a coupler of through port transmission ϵ . A linear laser cavity uses mirrors to create a feedback signal across a straight stretch of active fiber.

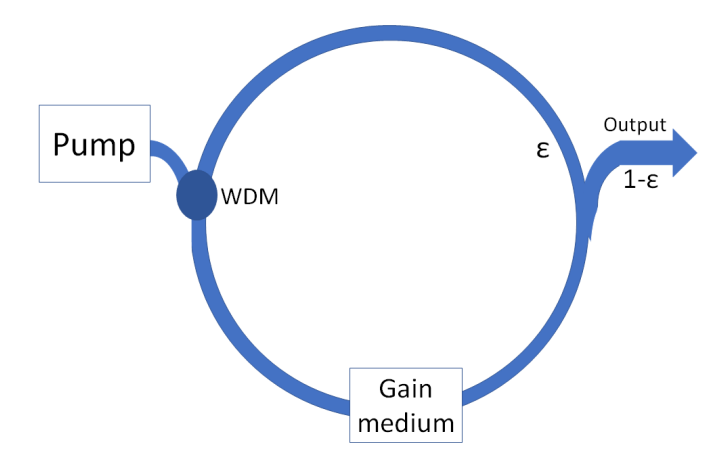


Fig. 2.8 Basic diagram of a circular ring cavity laser where ϵ is the through port coupling coefficient.



Fig. 2.9 Basic diagram of a linear cavity laser where R1 and R2 are input and output mirrors respectively.

Figure 2.10 shows how these laser cavities can be represented as a positive feedback system where G, L, and R are the gain, losses, and reflection experienced by the signal.

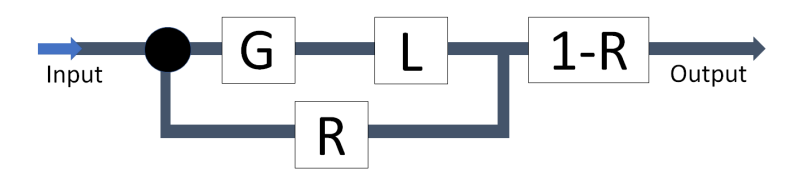


Fig. 2.10 System diagram of how a laser operates. G, L and R represent signal gain, loss and reflection coefficient respectively.

The gain coefficient can be matched with the stimulated emission equation given in 2.12. Notice the magnitude of gain (G in figure 2.10) is proportional to $N_2 - N_1$ also known as the population inversion between energy levels N_2 and N_1 . Population

inversion can be achieved by energizing electrons into N_2 through the absorption of pump photons of energy $\Delta E > \frac{hc}{\lambda_S}$ which can happen if $\lambda_P < \lambda_S$ or in a special case $\lambda_P > \lambda_S$ with excited state absorption processes (ESA) where λ_P, λ_S are the pump and signal wavelengths respectively. The losses (L in figure 2.10) comprise of the signal attenuation in propagation and splicing losses (fiber to fiber connections). Finally the reflection (R in figure 2.10) is the feedback of the signal into the laser medium and the compliment (1-R) the fraction of signal power leaving the cavity. A laser reaches steady state when the overall gain experienced by the signal including losses (L) and cavity output losses through a full feedback cycle is zero. This must occur in any laser system because if the pump input remains constant, the signal can only grow until it begins to significantly counter the population inversion established by the pump, at the limit of which the signal gain tends to zero.

2.2.6 Laser levels

With the concept of population inversion in mind, there are three typical laser transition structures that involve two, three, or four energy levels. These laser level schemes are shown in figure 2.11. A 2 level laser has a pump that brings electrons to the metastable (upper) energy level, which rapidly decays to fill up the lower energetic sub-bands, and lases to the ground state. The 3 level scheme pumps into the highest energy level, quickly decay non radiatively into the second energy level, and from there lase down to ground state. Finally, the 4 level laser pumps into the fourth energy level and subsequently a rapid decay brings it to the upper laser level, from there there is a laser transition from N_3 and N_2 and non-radiative decay into the ground state. The 4 level scheme is the most efficient because the ground state is typically highly populated and thus does not make for a good lower laser level [13].

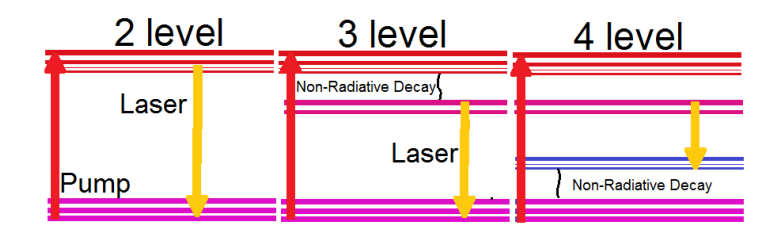


Fig. 2.11 Different kinds of laser schemes, with colors representing the population at that level (red is high population density, blue is low population density).

2.2.7 Physics of Er³⁺ ZBLAN

The physics of a laser operation depends on the choice of pump wavelength and host material. In this case, the host material is ZBLAN because of the fact that it has low losses in the mid-infrared due to low average phonon energies compared to silica based fibers, allows the upper laser level to have a longer lifetime which is beneficial to lasing [2]. The upper laser level for the required 2.7 μ m wavelength transition is ${}^{4}I_{11/2}$ and the corresponding lower laser level is ${}^{4}I_{13/2}$. As for the choice of pump wavelength, there are two viable options available: 980 nm and 790 nm wavelengths. The physics behind pumping at these wavelengths will now be discussed.

2.2.8 Pumping at a Wavelength of 980 nm

Figure 2.12 is the erbium energy level diagram with the relevant transitions for 980 nm pumping. The 980 nm wavelength pumps straight into the upper laser level at ${}^4I_{11/2}$. The lower laser level at ${}^4I_{13/2}$ is not ideal for laser operation due to its longer intrinsic lifetime of 9 ms compared to 6.9 ms which means that in steady state the upper laser level decays quicker than the lower in a manor that counters population inversion. More favorably however, the erbium atoms have ETU processes that transfer energy out of the lower laser level into higher energy states where they can possibly be stimulated to produce a second signal photon. This process is shown in figure 2.13.

By the absorption of one pump photon, and the subsequent emission of one signal photon, a chain reaction can occur where an ETU process brings a lower level laser electron back to the upper laser level without having to absorb another pump photon. This process leads to a geometric result, where the number of signal photons that come out of the pump is 2x as depicted in figure 2.13 [2]. However, not shown in the energy level diagram, but shown later in 4.3 is that there is an ESA from the upper laser level which excites electrons into the $^4S_{3/2}$ energy level which has a chance to emit 550 nm green fluorescence, consequently shorting the geometric series of ETU processes. Furthermore, this upper laser level ESA only gets more significant as pump power increases, especially in low doped fibers, because the ground state population depletes, and by equation 2.11 less pump photons are absorbed by the ground state hence more in excited states. In addition, ETU processes are proportional to the square of the energy level population they deplete (N^2) hence at low concentrations, are less effective. If the fiber is highly concentrated, this problem is not significant, and the ETU processes dominate.

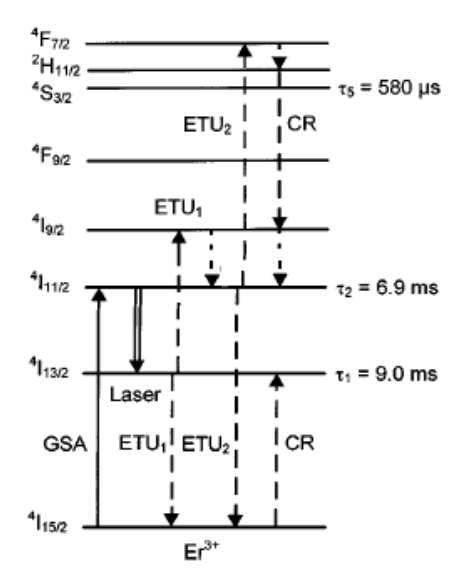


Fig. 2.12 Important energy level diagram showing transitions with 980 nm pumping [2]

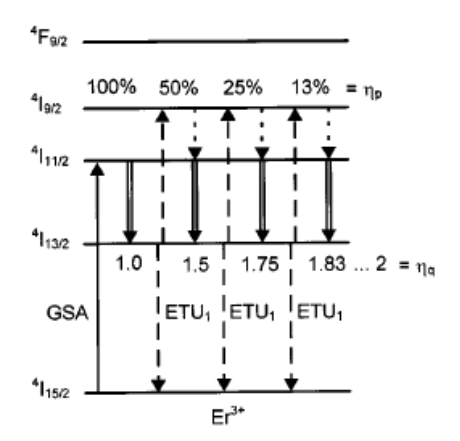


Fig. 2.13 980 nm pumping energy levels showing how ETU process increases efficiency. [2]

2.2.9 Pumping at a Wavelength of 790 nm

The energy level scheme for 790 nm pumping is shown in figure 2.14. This pumping method is a 4 level laser. The pump excites electrons into the ${}^{4}I_{9/2}$ level, which then decay rapidly into the upper laser level and generate a signal photon from there. A positive aspect of this pumping regime is that the lower laser level has a strong ESA which depletes it, in effect alleviating the long lifetime issue. However, since the ESA is so strong from the lower laser level, ETU processes are not very important and thus the energy recycling which makes the 980 nm pump so efficient is not so active here. Similarly to the 980 nm pump, there is an ESA from the upper laser level not shown in this diagram, however is shown in figure 4.2 later on. However, in this case, the ESA from the upper laser level is an order of magnitude less potent than the ESA from the lower laser level as seen in figure 2.15 and hence population inversion remains strong even at low erbium concentrations. In fact, the 790 nm pump thrives when the ground state is nearly depleted known as ground state bleaching. As such in low doped, core pumped fibers with small core radii, the 790 nm pump has had the best results [2]. Despite the positive results, there is an issue of output power saturation when pump powers are too high due to the onset of lasing at 850 nm, which fills up the lower laser level of the 2.7 μ m transition. One way to relieve this issue is to use mirrors that surpress the 850 nm transition, this was done in [16].

Another beneficial aspect of the erbium 2.7 μ m wavelength transition is that it does not need actual population inversion to get gain at the signal. This is because according to [2] there are Stark splittings in the upper and lower laser levels that contribute to population inversion. The equation for stimulated emission at 2.7 μ m is show below 2.12.

$$R_{SE} = \frac{\lambda_S \Gamma_S \sigma_{se}}{hc A_{eff}} [b_2 N_2 - \frac{g_2}{g_1} b_1 N_1] P_S$$
 (2.13)

Where $b_1 = 0.113$, $b_2 = 0.200$ are the Boltzmann factors of the lower and upper levels

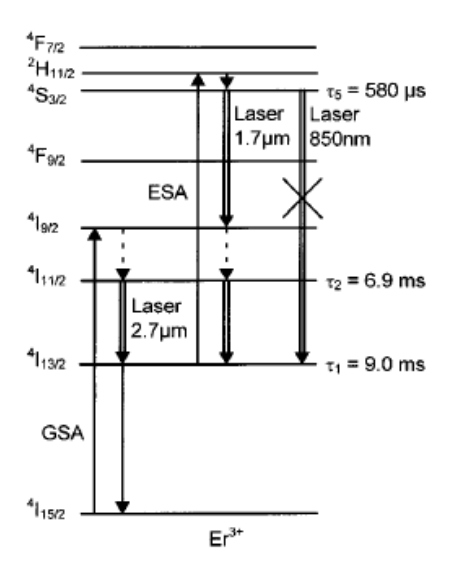


Fig. 2.14 Energy level diagram with relevant processes when pumping with a wavelength of 790 nm. [2]

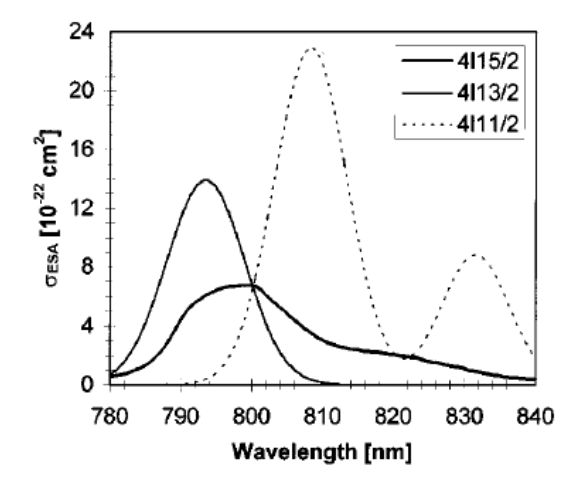


Fig. 2.15 Measured Erbium absorption crossections from around the wavelength of 790 nm. Note the order of magnitude difference between absorption from the upper laser level ${}^4I_{11/2}$ compared to the ESA from the lower laser level ${}^4I_{13/2}$ [2].

respectively, and the Kramer's degeneracies $g_1, g_2 = 2$ [12]. These values satisfy the following CW inversion condition, which means the population levels $N_2 < N_1$ can still provide signal gain.

$$\frac{b_2 \tau_2}{\beta_{21} b_1 \tau_1} > 1 \tag{2.14}$$

Using the parameter values from [15]: $\beta_{21} = 0.370$, $\tau_1 = 9$ ms, $\tau_2 = 6.7$ ms thus the ratio needed between N_2 and N_1 is $\frac{.2*6.7}{0.37*0.113*9} = 3.561$. Therefore, the steady state population of N_2 can be three and a half times less populated than N_1 and still impart a positive gain on the 2.7 μ m signal.

Chapter 3

Fluorescence Measurements

In this chapter, the experiments performed throughout the thesis duration are presented and analyzed in depth. The experimental portion of this research is comprised of two main experiments which use Er-doped ZBLAN as the active gain medium: a fluorescent source, and a free-space coupled linear laser cavity. The fluorescent source experiment is designed to determine if there is evidence of a 2.7 μ m signal through 790 nm or 980 nm wavelength pumping, and further which of the two produces the most promising results. The second experiment is intended to build on the first and produce a laser at 2.7 μ m, however this design is unsuccessful despite several attempts. It is concluded that inherent flaws in the ZBLAN fiber's dimensions cause it to be impractical for the kind of free-space coupled linear cavity proposed in the design. Finally, a new ZBLAN fiber is proposed with design improvements with respect to the old one.

3.1 Fluorescence Experiment

This experiment consists of measuring the resulting fluorescence from a 4.9 μ m core diameter, 2000 ppm Er³⁺ - ZBLAN fiber with an NA of 0.21 and length of 5 meters through a direct coupling connection with 790 nm or 980 nm wavelength laser diodes. The purpose of this experiment is to study the resulting spectrum and fluorescence power from the fiber in order to understand the Er³⁺ energy level mechanics as it pertains to emission at a wavelength of 2.7 μ m and use those results to conclude which wavelength is optimum. Although the differences between the pumping wavelengths 790 nm and 980 nm have been studied previously, there are no direct comparisons between the two in literature, especially for fibers of similar concentration and dimensions. The experimental setup is displayed in figure 3.1 below.

3.1.1 Fluorescence Source Design

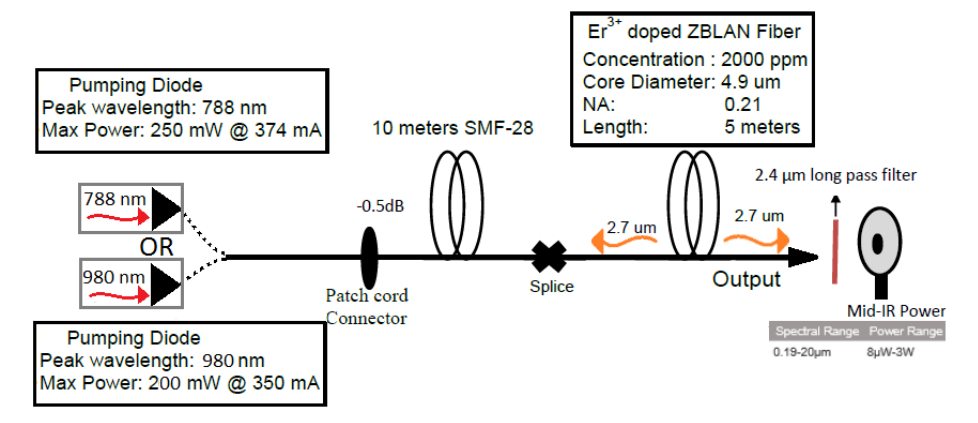


Fig. 3.1 The experimental set-up of an Er^{3+} - ZBLAN fiber fluorescent source.

The fluorescent source is composed of 3 sections: a pump diode of either 980 nm or 790 nm wavelength, a 10 m stretch of SMF-28 fiber, and an active medium of Er³⁺ doped ZBLAN fiber. The 980 nm and 790 nm pumps are designed to operate at a maximum power of 200 mW and 250 mW respectively. The SMF-28 section is placed

to attenuate the 2.7 μ m backward ASE in order to protect the pump diodes and keep their output stable. Next, the 2000 ppm Er³⁺ ZBLAN fiber is cleaved through a polishing method and spliced to the SMF-28 with UV reactive glue to maintain the connection. Finally, the output is sent through a longpass filter which blocks wavelengths below 2.4 μ m and transmits 90% of power between 2.4 μ m and 5 μ m, and measured with a power meter that has a broad 0.1 - 20 μ m spectral range and dynamic power range of 8 μ W up to 3 W.

3.1.2 Coupling Efficiency Discussion

It is important to discuss coupling losses in the system in order to know how much launched pump power is inserted into the ZBLAN fiber. Since both the pump sources operate in single mode, equation 2.4 can be used to determine the mode coupling efficiency. Using the respective normalized frequency V for both fibers with Eq 2.2, it is found that the beam radius at both wavelengths 980 nm and 790 nm are equal to 2.1 μ m and 3.35 μ m for ZBLAN and SMF-28 respectively. Using these radii for w_1 and w_2 it is determined the theoretical mode coupling ratio is $\eta = 80.1\%$. By the same calculations, the beam radii for 1310 nm are 2.8 and 4.6 for ZBLAN and SMF-28 respectively, leading to an efficiency of $\eta = 79.1\%$. Due to non idealities in experimental mode coupling resulting from translation stage alignment errors, the true value of η is expected to be lower. To have a more precise idea of the pump to ZBLAN fiber coupling efficiency, a 1310 nm signal was used which has low loss ($\approx 150 \text{ dB/km}$) in Er³+ doped fibers as seen in figure 3.2. This attenuation over a length of 3.5 m amounts to a small 0.5 dB overall loss.

Total Power at 1310 nm	1.1 mW
Output power through 3.5 m ZBLAN	$570~\mu\mathrm{W}$
Output power through 25 cm ZBLAN	$575 \ \mu W$

Table 3.1 The measured output signal power at a wavelength of 1310 nm used to determine the mode coupling efficiency experimentally.

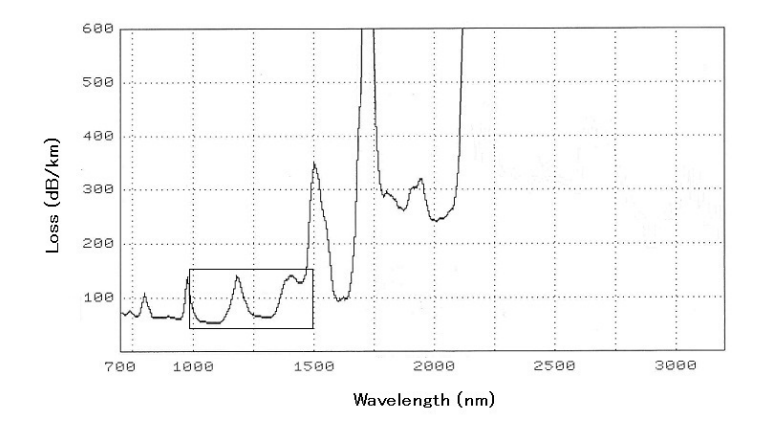


Fig. 3.2 The loss spectrum of the erbium doped ZBLAN fiber provided by the manufacturer Fiber Labs. Note the window showing losses between 1000 nm and 1550 nm.

As seen in table 3.1, despite a 3.25 meter difference in length between the two test fibers, a 5 μ W change in received power is noticed at the output. Thus, as expected the bulk of losses do not happen due to light attenuation, instead the loss is dominated by the coupling efficiency. By this logic, an estimate for the experimental coupling efficiency at 1310 nm is $\eta = 52\%$. This decreased percentage from the expected 79.1% can be attributed to non-ideal polishing of the fiber or slight misalignment to the SMF-28. Figure 3.3 depicts a direct coupling scenario where a small difference dx in proximity causes some loss from beam divergence. Notice also the definition of launched versus inserted power, launched is the total power being sent from an input light source, while inserted power is how much of that light is guided in the target optical fiber, in this case a ZBLAN fiber.

3.1.3 Fluorescence Results

With the mode coupling efficiency known, a relationship can be established between the launched pump power and power inserted into the fiber. Table 3.2 shows the inserted pump powers of each 790 nm and 980 nm wavelengths for the fluorescence experiment.

The output beam was sent through an OSA (Optical Spectrum Analyzer) to mea-

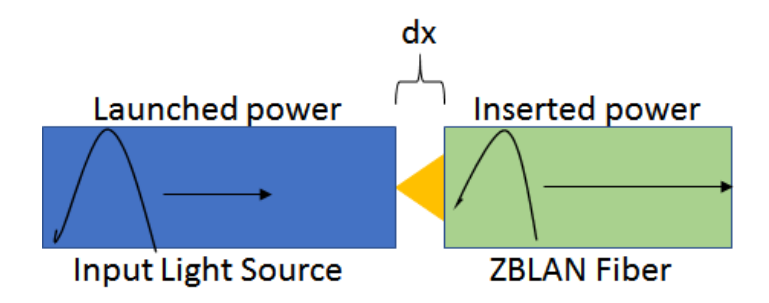


Fig. 3.3 An example of direct coupling between two fibers depicting the difference between launched and inserted power. Notice within the small alignment error dx there is some loss of light.

Pumping Wavelength (nm)	790	980
Launched Pump Power (mW)	215	200
Inserted Pump Power (mW)	107	100

Table 3.2 Summary of the launched and inserted pump powers for the fluorescence spectrum experiment. Measurements made by using power meter detailed in Figure 3.1.

sure the resulting ASE spectra. The results show in figures 3.4 and 3.5 are normalized with respect to each other such that the peak power of the 2.7 / mum fluorescence in the 790 nm wavelength pumping scheme is unity.

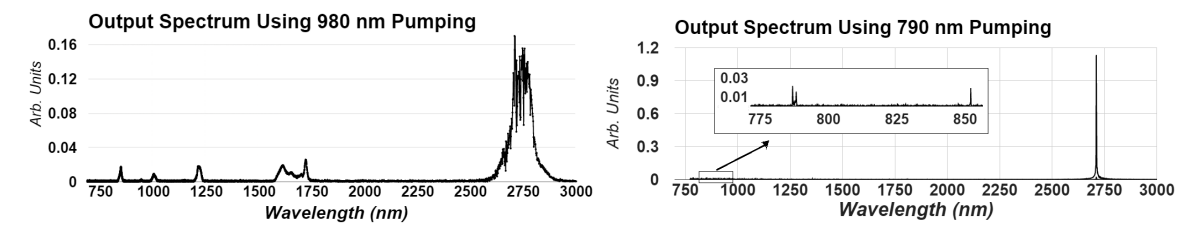


Fig. 3.4 Linear scale spectral results of the fluorescence experiment using a 980 nm pump signal

Fig. 3.5 Linear scale spectral results of the fluorescence experiment using a 790 nm pump signal.

The most striking aspect when making a comparison of the two spectra is the difference in line width. ASE resulting from 980 nm pumping has a broad output spectra centered at 2750 nm and covers a band from 2650 nm to 2800 nm. Furthermore, the output has other spectral components, specifically at 850 nm, 1000 nm,

1220 nm, and 1600 nm - 1750 nm. In contrast, the resulting output from the 790 nm pump is nearly exclusive at 2710 nm with a narrow line width of approximately 4 nm, with no competing signals at other wavelengths except a trace of the residual pump at 790 nm and slight signal at 850 nm. Indeed the output spectrum resulting from using 790 nm pump exhibits the spectral characteristics of a laser, even though the only feedback for the 2.7 μ m signal is from Fresnel reflections of approximately 4% at each fiber end.

In accordance to the difference in spectra, the average power measurements favor the 790 nm pump. A rough measurement of average power was made by placing the longpass filter in front of the exit end of the ZBLAN fiber, and placing the power meter as close as possible to it. With this measurement method, there is a significant amount of signal power that can escape through beam divergence, hence the measured powers are not accurately indicative of true output power. However, since the same method was used for both pump trials, there is meaning in comparing the two numbers, as they were both subject to the same uncertainty. The output signal measurements are summarized in the table below.

Pump Wavelength (nm)	790	980
Total Power at Output (mW)	13	6
$2.7 \ \mu \text{m}$ signal power measured (μW)	250	60

Table 3.3 Summary of the total fluorescence measured and power at 2.7 μm for the fluorescence experiment. Measurements made by using power meter detailed in Figure 3.1 using a long pass filter for isolated 2.7 μm power.

The total output fluorescence is everything from the output end of the fiber with no filters, thus it contains the entirety of ASE's as well as the residual pump. From figures 3.5 and 3.4 it can be determined that within the 750 nm - 3000 nm wavelength band, the generated 2.7 μ m signal dominates all others. However, a quite strong green fluorescence is observed at 544 nm as a result of a spontaneous transition from the

 $^4S_{3/2}$ to ground state which does not fall within the spectral range of the detector. Thus most of the 13 mW (790 nm) and 6 mW (980 nm) total output power is believed to be a result of the 544 nm fluorescence, figure 3.6 demonstrates the strong green glow when the set-up is in action.

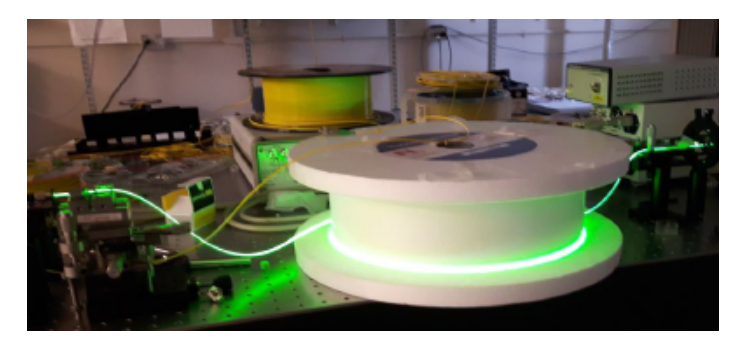


Fig. 3.6 the fluorescence experiment, left hand side shows the pump direct coupled to the input of a 5m $\rm Er^{3+}$ ZBLAN fiber

In order to understand why the spectrum and generated 2.7 μ m power drastically depend on the use of pump wavelength, we must look into the Erbium energy level models for each wavelength. Figure 3.7 shows the important energy transitions for each wavelength with a colour code to visualize which energy levels are most populated in each scheme. Both wavelength transitions will now be discussed separately and then related to one another.

In the 980 nm wavelength pumping scheme, it is not surprising to see that there is a broader output around the 2700 nm mark because the GSA sends electrons directly into the upper laser level which fills many sub-bands. Each sub-band has its own distinct wavelength when it transitions down to the lower laser level, which causes a broader output in ASE around 2700 nm. Further, since the only ESA happens from the upper laser level, and the lower laser level relies on ETU1 to be emptied. The population inversion is overall weaker than in the 790 nm case, thus explaining the lower output power at 2.7 μ m. In addition, the small core diameter of 4.9 μ m combined with the low concentration of 2000 ppm causes ground state bleaching to occur [2] due to the high pump intensity rapidly exciting most of the ground

state electrons. Subsequently, most pump absorption occurs in excited states further contributing to the upper laser level clearance. Moreover, since the upper laser level is being cleared by both ETU2 and ESA which excite electrons into the ${}^4S_{3/2}$ level, both the 850 nm and 1700 nm transitions are stimulated as evidenced by the corresponding peaks in figure 3.4.

The 790 nm wavelength pumping scheme yielded much more potent gain at the signal wavelength of 2.7 μ m, so much so that it lased through Fresnel reflections alone. Much like in the 980 nm case, the characteristics of the fiber cause GSB which lead to more prevalent excited state absorption. In this case, there are two possible absorptions, either in the upper laser level (ESA2) or lower laser level (ESA1). The ESA1 crossection is an order of magnitude larger than that of ESA2 [2], thus GSB is beneficial to lasing. Furthermore, both ESA's contribute to the ${}^4S_{3/2}$ level and generate 544 nm green fluorescence as well as 850 nm light.

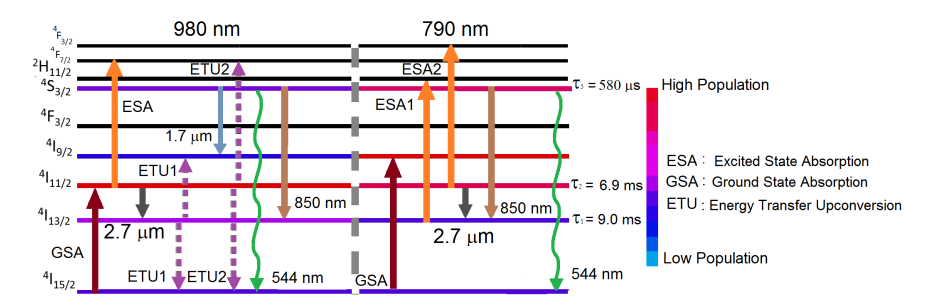


Fig. 3.7 Energy level diagram showing the relevant energy transitions for 980 nm and 790 nm pumping, color coded for suspected population levels. Energy levels and transitions are based on [2] [17]

From the analysis it is clear that for the conditions of the ZBLAN fiber studied, and the relatively low pump power used, the 790 nm pump is advantageous. However, it is known from [17] that a similar fiber of core diameter 6.5 μ m and Er concentration 5000 ppm exhibits output saturation at 790 nm pump powers of over 500 mW, due to the 850 nm transition lasing and filling up the 2.7 μ m signals lower laser level. Since the inserted pump power is not much over 100 mW, the 790 nm wavelength pump is superior.

In order to investigate further the energy transfer from pump to 2.7 μ m signal, as well as study the gain profile from the upper laser level, consider figure 3.8

.

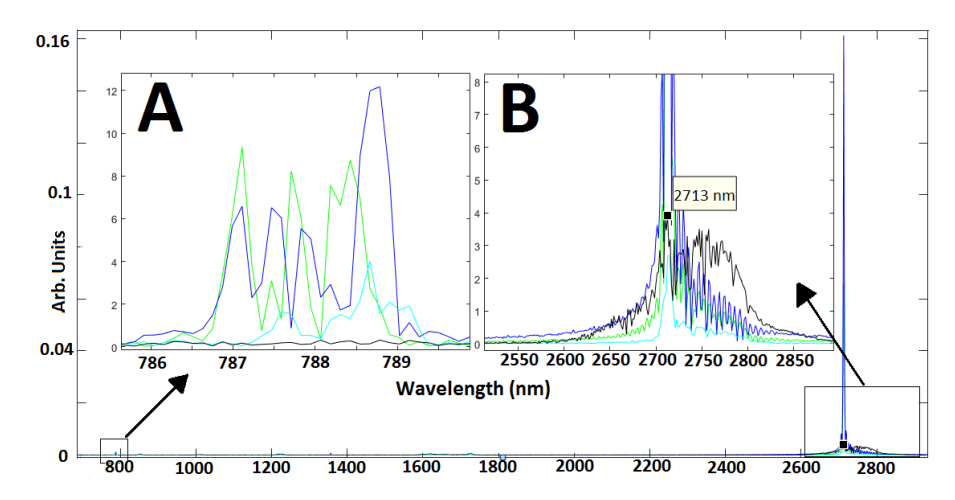


Fig. 3.8 Output Spectrum for varying 790 nm pump powers superimposed with the 980 nm pump output spectrum. Green: 75 mW, Blue: 85 mW, Cyan: 35 mW, Black: 100 mW of 980 nm. Note: powers listed are inserted powers A. Residual Pump. B: $2.7~\mu m$ signal

Part A of figure 3.8 shows the residual 790 nm pump at the output of the ZBLAN fiber. It is interesting to see which wavelengths get more absorbed than others based on the inserted power difference. Specifically, the peaks on the figure show where the pump is less absorbed and surprisingly the location of the peaks are not always constant. This lack of consistency could be evidence of ESA processes and ground state bleaching. For instance, according to the absorption crossections for Er in ZBLAN in figure 2.15, both ESA1 and GSA are supposed to get stronger as the wavelength approaches 790 nm. However, it is clear that at the highest pump power shown here (blue) that the least power overall is absorbed close to 790 nm. This must mean that both the lower laser level and the ground state are insignificantly populated relative to the upper laser level, and thus a large portion of the absorption occurs at the upper laser level, which as previously stated, has a crossection one order of magnitude lower than the others. This is actually a good sign from an

optical amplifying perspective because it means that the lower laser level is sufficiently cleared relative to the upper, which means stimulated emission dominates throughout the fiber.

Part B of figure 3.8 shows how the 2.7 μ m signal changes as the pump is increased. Also included in the graph is again the resultant 980 nm pump spectrum to be used as a reference for the gain profile of emission from the upper laser level. At a low pump power of 35 mW (cyan), we get a glimpse of the ASE profile from the 790 nm pump before the 2.7 μ m signal dominates totally the closely surrounding ASE. Notice there is an absence of ASE to the left of the dominating 2713 nm wavelength, and to the right, a small fluorescence is present stretching to 2800 nm. As the pump increases, the same trend continues, most of the extra ASE remains to the right of the 2713 nm peak, however it becomes more and more dominated by the 2713 nm emission. When pumping with the wavelength of 980 nm, the peak emission is still at 2713 nm, however the emission on the right side remains relatively strong. From this phenomenon we can draw two separate conclusions: 1. The gain profile from the ${}^4I_{11/2} \rightarrow {}^4I_{13/2}$ is broad and peaks at the wavelength of 2713 nm. The rapid ion quenching from ${}^4I_{9/2}$ favors the sub-band of ${}^4I_{11/2}$ responsible for emission at 2713 nm. Both these points together explain why the 2700 nm signal has much greater gain with 790 nm pumping.

3.2 Er³⁺ ZBLAN Free-Space Pumped Laser

After seeing promising results with the fluorescent source, the next step was to add feedback mirrors to create a laser cavity for the 2.7 μ m signal to achieve higher output powers. Figure 3.9 below is the design of the free-space linear laser cavity.

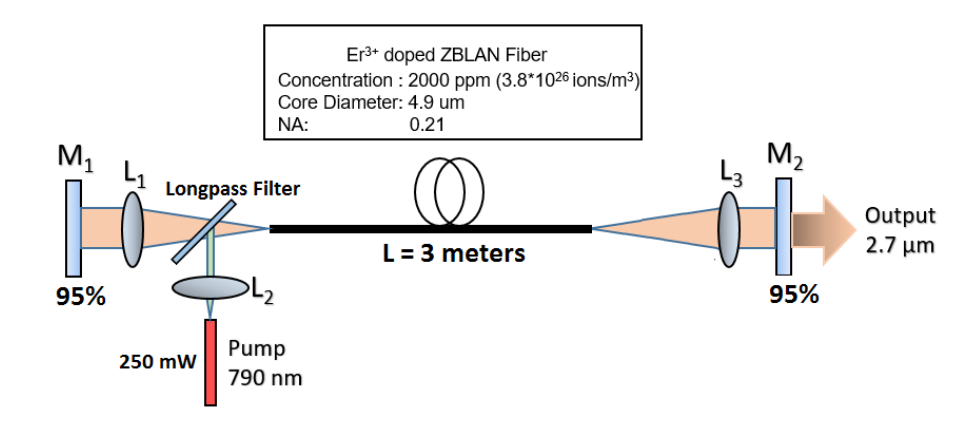


Fig. 3.9 Linear free-space coupled laser cavity

3.2.1 Linear Free-Space Pumped Set-up

The original design for the linear laser cavity consisted of 3 lenses, two 95% mirrors, a 2.4 μ m longpass filter, and a 790 nm pump source. The longpass filter was used as a dichroic mirror for 790 nm and 2700 nm. Hence the filter reflected the pump signal into the fiber whist allowing the 2.7 μ m signal to pass through and be fed back into the fiber by a 95% reflecting mirror. The length of the ZBLAN fiber has gotten shortened to 3 m due to a break that occurred in the 5 m fiber. The weakness of the ZBLAN glass is one of the downsides that will be discussed later. Next we discuss the losses in the system.

3.2.2 Loss Analysis

To measure the losses, the pump was sent through each section individually while keeping track of the launched and received power. The results are summarized in table 3.4 below:

Component under test	Lenses	Longpass filter
Pump Power (mW)	193	193
Output Power (mW)	150	95
Loss (dB)	1	3.1

Table 3.4 Loss in the free-space portion of the laser cavity

As can be seen in from the table above, losses are a major problem in the free-space set-up. the total losses incurred by the pump by the time it reaches the ZBLAN fiber entrance is 4.1 dB, that means only about 80 mW would have a chance to enter the fiber if the pump signal started off at 200 mW. Clearly, the biggest source of loss at just over 3 dB is the longpass filter, which was initially assumed to be highly reflecting at the pump wavelength. With these losses, the best output fluorescence that could be achieved was just over 6 mW at a launched pump power of 200 mW. Since the fiber that was previously worked with for the fluorescent source was 5 m long, the direct coupling experiment was redone to find out what is expected at the output. Figure 3.10 below shows the fluorescent results with direct coupling (orange), free-space coupling (blue) and the threshold at which a 2.7 μ m signal could be easily detected.

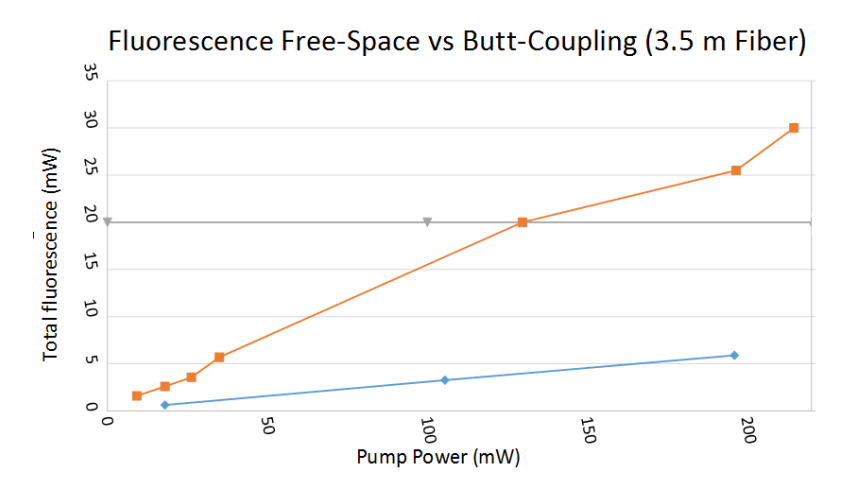


Fig. 3.10 Comparison of output fluorescence while using direct coupling (orange) and free-space coupling (blue). the grey line depicts a threshold fluoroescence value where 2.7 μm could be first detected

Given the heavy losses, in the best achieved scenario with free-space coupling, only 24% of pump power was coupled into the ZBLAN fiber as compared to direct coupling. An interesting comparison to demonstrate the difference in coupling power between free space and direct coupling is given in figures 3.12 and 3.11. Notice how much more intense the green glow is in the direct coupling case. Note, the green fluorescence is a result of a high population in the ${}^4S_{3/2}$ energy level, which is a result of ESA processes meaning the pump is well absorbed.

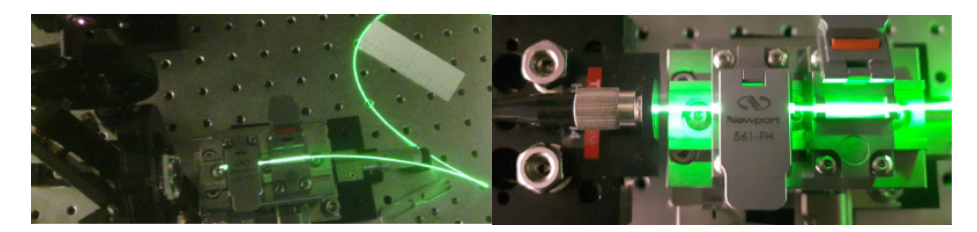


Fig. 3.11 Example of best achieved free space coupling given all the losses.

Fig. 3.12 Much more powerful direct coupling is giving an intense green glow

3.2.3 Forward and Backward Pumped Laser

With limited pump power, lasing could not be observed. In an attempt to resolve this issue, a more powerful pump at 790 nm with a max power of 450 mW was added to the set-up in a backward pumping configuration as shown in figure 3.13.

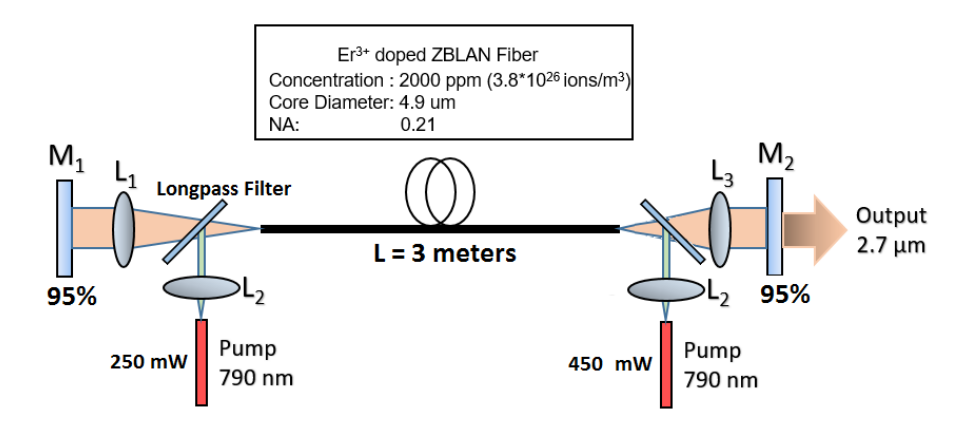


Fig. 3.13 New design with forward and backward pumping to resolve the loss issue

In this configuration, the maximum total launched pump power is 700 mW, and thus with the losses discussed previously of 4.1 dB, the total possible inserted power is 272.3 mW. With 24% conversion efficiency from direct-coupling to free-space coupling, at least 65 mW of total pump power is expected to be inserted into the fiber, which is known to be enough to generate a 2.7 μ m signal. However, due to divergence of the 2.7 μ m signal, L₃ did not capture enough light to be fed back into the ZBLAN fiber. Thus enough feedback was never achieved to get a working laser.

3.2.4 Fiber Issues

After many failed attempts to make a free-space laser cavity like those shown in figures 3.9 and 3.13, it was decided that a ZBLAN fiber of these dimensions is impractical for free-space pumping designs. Specifically, the characteristics of the fiber cause three main problems: 1. fragility 2. large beam divergence 3. Low coupling efficiency. ZBLAN glass is acutely susceptible to sheer stress and despite its protective coating, can still form internal cracks based on slight mishandling or pressure from fiber clamps. In addition, the small core diameter of 4.9 μ m makes the problem worse because compressive stress is converted to sheer stress more easily. Due to fragility, it is a common occurrence for the fiber to break in close proximity to where it is being held down in a translation stage. The second issue is due to an amalgamation of the small core radius $(2.45 \ \mu m)$ and high NA (0.21). In Gaussian beams it is known that divergence is proportional to the initial beam waist. A large NA only enhances the problem by increasing the V number, hence by equation 2.2 the beam waist size is reduced, and divergence is increased by decreasing beam waist by equation 2.5. The high NA of 0.21 could be considered an asset ove when considering pump to ZBLAN coupling because the acceptance angle is large, however the 2.7 μ m signal will also have a high divergence angle when exiting the fiber making it difficult to capture in a lens. Thus the benefit of increased pump coupling is outweighed by the con of not

being able to feedback the laser signal. Finally, the third problem is lack of free-space coupling efficiency. Again, the small core radius is at fault. It is difficult enough to couple light into a small core, however what further enhances this difficulty is the susceptibility of a small fiber to tensions which tend the fiber to bend. When removing the ZBLAN fiber's protective coating in preparation for polishing, a random tension is imprinted on the fiber causing it to bend in a favored direction. When placing the fiber for free-space coupling, the tension causes the fiber tip to never be perpendicular to the incident light. Controlling the angle with a yaw-pitch tool, which gives precise control on the angular orientation of the fiber as shown in 3.14, is still impractical because the random angle changes each time the fiber is removed and placed back. Since in the free-space coupled design, both the pump and the laser signal are to share the same path, exact alignment is imperative for both paths. If a yaw-pitch adjustment is to be made to cater to the pump, the laser signal loses alignment and vice versa. Due to this reasoning, despite the promising results of the fluorescence experiment, a ZBLAN fiber with such a low core radius is not practical for free-space pumping. Instead, an all-fiber solution is more appropriate using fiber bragg gratings for signal feedback. Typical couplers could not be used because silica glass absorbs at the wavelength of $2.7 \mu m$.

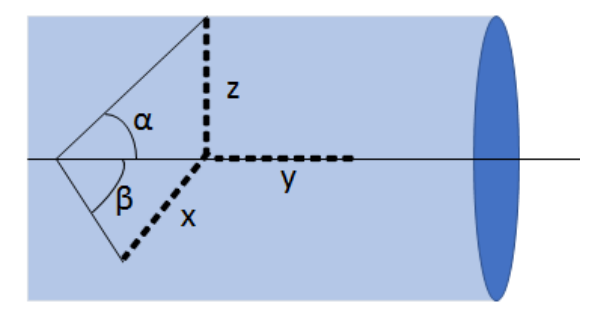


Fig. 3.14 Diagram of a fiber showing the yaw (β) and pitch (α) axis used for angular alignment

3.2.5 Suggestions and Conclusions

Since the issues with the design are mostly due to the choice of ZBLAN fiber, it is recommended to change the fiber characteristics. A good candidate fiber currently on the market, which is used in [18] [19], has the following characteristics summarized in table 3.5:

Core Radius (μm)	NA	Clad type	Er ³⁺ concentration (ppm)
15	0.12	double clad D-shape	70000

Table 3.5 Suggested ZBLAN fiber characteristics

It is believed that the flaws of the current ZBLAN fiber are all resolved with this proposed choice. Each concern is addressed with these new fiber characteristics. The first, which is fragility, is corrected for because the larger core diameter (15 μ m) and the double clad increases the overall thickness of the fiber which makes it less susceptible to breaking from compression, or fiber clamps. The second concern of divergence is handled as well because the core radius is larger and the NA is smaller and thus the Gaussian beam at the signal wavelength diverges at a slower rate. Lastly, coupling efficiency is also superior with this design because the core radius is larger, and in the event a portion of light escapes the core, the double clad will ensure not all light is lost. In addition, the increase in core radius is accompanied by a much higher erbium concentration (35 times more), thus there is a net increase of erbium ions that can interact with the pump. A complete picture of how the two fibers compare is displayed in tables 3.6 and 3.7.

The mode radius and effective mode area are important design parameters for both the pump and signal because they determine the physical overlap within which stimulated emission or absorption processes can take place. To get a more quantitative idea of the benefits of using the new fiber design, we can compare how more signal

 $70000 \text{ ppm Er}^{3+} \text{ ZBLAN fiber}$

Wavelength: λ (nm)	790	980	2700
Normalized frequency: V	7.15	5.77	2.09
Mode Radius*: w_0 (μ m)	5.51	5.75	9.19
Effective Mode Area*: A_{eff} (μ m ²)	109.5	117	240.8
Power Confined in Core*: P_{core} (%)	99	98.2	77.2

Table 3.6 Mode characteristics at each wavelength of interest. *values for LP01 mode only

 $2000 \text{ ppm } \text{Er}^{3+} \text{ ZBLAN fiber}$

Wavelength: λ (nm)	790	980	2700
Normalized frequency: V	4.09	3.298	1.2
Mode Radius*: w_0 (μ m)	2.07	2.25	4.61
Effective Mode Area*: A_{eff} (μ m ²)	14.4	16.5	114.8
Power Confined in Core*: P_{core} (%)	95.5	92.1	32.9

Table 3.7 Mode characteristics at each wavelength of interest. *values for LP01 mode only

and pump photons are available for stimulated emission and absorption respectively. From equations 2.11 and 2.12, and using table 3.7 and 3.6 for A_{eff} , we find the ratio of $\frac{R_{SE_{70000ppm}}}{R_{SE_{2000ppm}}} = 0.816 \left(\frac{N_{2,70000ppm}-N_{1,70000ppm}}{N_{2,2000ppm}-N_{1,2000ppm}}\right)$ and $\frac{R_{P_{70000ppm}}}{R_{P_{2000ppm}}} = 0.478 \frac{N_{0,70000ppm}}{N_{0,2000ppm}}$. These ratios depend on the population levels, and thus in order to get an accurate picture of how the two fibers compare, simulations need to be performed. These are done in the next chapter. For now it is suffice to say that the ratio's are likely to be over 1 since the ratio of 70000/2000 is a factor of 35. If we assume all power is absorbed from the ground state, we can expect $R_{P_{70000ppm}}$ to be 35*0.478 = 16.73, which means it would take only 30 cm to absorb the same amount of pump as 5 m of the 2000 ppm fiber, as a first order approximation. Since one of the goals of this research is to achieve a compact laser design, the 70000 ppm fiber shows good promise.

Chapter 4

Modeling

The optimization of physical parameters leading to functional laser requires an efficient model. In this section, a model is described in detail and simulation results are compared to their experimental counterparts in the previous chapter in order to determine the validity of the laser model parameters. Once the parameters are consistent with experiment, predictions are made for an optimized laser design.

4.1 Simulation Description and Assumptions

In order to simulate the operation of a laser cavity, it is required to work in the dimensions of both time and space. Specifically, time domain to solve rate equations and spacial domain to update and propagate all necessary signals. The simulation method used here closely resembles what is done in [12], however the model parameters are taken from [17] [15] [20]. First, the results from [12], where the simulations and rate equations are for 980 nm pumping only, were replicated to ensure the accuracy of the program. Next, the specific parameters for 790 nm pumping as well as the rate equations from taken from [17] and integrated into the validated simulation code to create a second program for 790 nm pumping. Finally, the simulations were run by changing the fiber parameters such as dopant concentration, length, and core

radius in both programs to obtain a model of the Er-doped ZBLAN for both pumping schemes and fiber characteristic scenarios. The simulation method is as follows: The fiber is split into N subsections as shown in figure 4.1 within which the pump and all signal powers are assumed constant. The simulation keeps track of 6 different signals (550 nm, 790 nm, 970 nm, 1550 nm, 1700 nm, 2700 nm) by keeping track of their respective spontaneous and stimulated emissions. Note, each signal consists of a single wavelength.

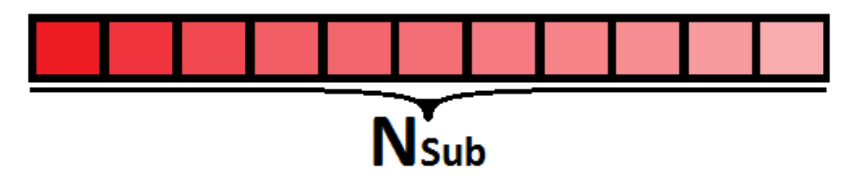


Fig. 4.1 Showing the fiber cut into N subsections with the red gradient representing the pump absorption.

In the time domain, the population rate equations are solved until they reach steady state starting with the initial conditions of inserted pump and signal powers. All erbium atoms are assumed to be in the ground state (N_0) level at t = 0. The population rate equations are given in the next page for both pumps respectively. Below are the energy level diagrams they are based on.

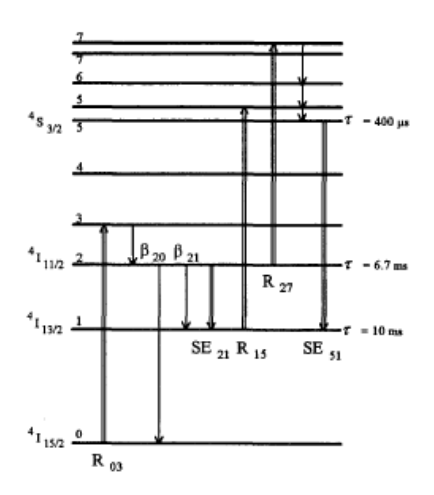


Fig. 4.2 Energy level diagram the 790 nm pump simulations are based on [17].

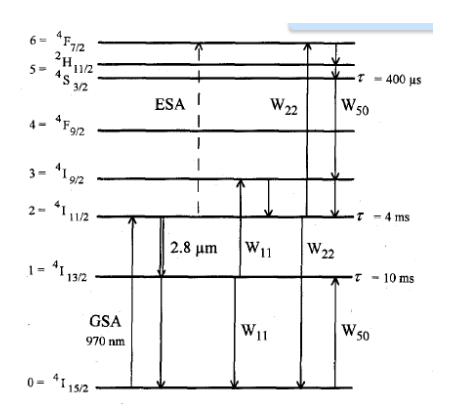


Fig. 4.3 Energy level diagram the 980 nm pump simulations are based on [12].

The rate equations for 980 nm wavelength pumping:

$$\frac{dN_6(z,t)}{dt} = R_{ESA}(z,t) - t_6^{-1}N_6(z,t) + W_{22}N_2^2(z,t)$$
(4.1)

$$\frac{dN_5(z,t)}{dt} = \beta_{65}t_6^{-1}N_6(z,t) - t_5^{-1}N_5(z,t) - W_{50}N_5(z,t)N_0(z,t)$$
(4.2)

$$\frac{dN_4(z,t)}{dt} = \sum_{i=5.6} [\beta_{i4}t_i^{-1}N_i] - t_4^{-1}N_4(z,t)$$
(4.3)

$$\frac{dN_3(z,t)}{dt} = \sum_{i=4,5,6} \left[\beta_{i3} t_i^{-1} N_i \right] - t_3^{-1} N_3(z,t) + W_{50} N_5(z,t) N_0(z,t) + W_{11} N_1^2(z,t)$$
(4.4)

$$\frac{dN_2(z,t)}{dt} = R_{GSA} - R_{ESA}(z,t) + \sum_{i=3,\dots,6} \left[\beta_{i2}t_i^{-1}N_i\right] - R_{SE}(z,t) - \tau_2^{-1}N_2(z,t) - 2 * W_{22}N_2^2(z,t)$$
(4.5)

$$\frac{dN_1(z,t)}{dt} = \sum_{i=2,\dots,6} \left[\beta_{i1} t_i^{-1} N_i(z,t) \right] - \tau_1^{-1} N_1(z,t) + W_{50} N_5(z,t) N_0(z,t) - 2W_{11} N_1^2(z,t) + R_{SE}(z,t) N_0(z,t) \right] + W_{50} N_5(z,t) N_0(z,t) N_0(z,t) + W_{50} N_5(z,t) N_0(z,t) N_0(z,t) N_0(z,t) + W_{50} N_5(z,t) N_0(z,t) N_0(z,t$$

(4.6)

$$N_0(z,t) = N_{Er} - \sum_{i=1}^6 N_i(z,t)$$
(4.7)

where N_i is the i^{th} energy level, R_{SE} is stimulated emission between energy levels N_2 and N_1 , and R_{ESA} , R_{GSA} are stimulated absorption from N_2 and N_0 respectively.

Branching Ratios

$\beta_{10} = 1.00$	$\beta_{54} = 0.34$
$\beta_{21} = 0.370$	$\beta_{51} = 0.18$
$\beta_{20} = 0.630$	$\beta_{50} = 0.44$
$\beta_{32} = 0.99$	$\beta_{65} = 0.941$
$\beta_{43} = 0.85$	$\beta_{60} = 0.059$
$\beta_{40} = 0.14$	$\beta_{76} = 1.00$
$\beta_{31} = 0$	$\beta_{30} = 0.01$
$\beta_{42} = .006$	$\beta_{41} = .004$
$\beta_{53} = .012$	$\beta_{52} = .015$

Intrinsic Times

$\tau_1 = 9 \text{ ms}$	$\tau_2 = 6.9 \text{ ms}$
$\tau_3 = 6.6 \ \mu \mathrm{s}$	$\tau_4 = 100 \; \mu \text{s}$
$\tau_5 = 400 \; \mu \text{s}$	$\tau_6 = 5 \ \mu s$

ETU Processes

$W_{22} = 3.6 \times 10^{-23} \ W_{22}$	$_{11} = 1.2 \times 10^{-23}$	$W_{50} = 2.7 \times 10^{-23}$
---	-------------------------------	--------------------------------

The rate equations for 790 nm wavelength pumping:

$$\frac{dN_7(z,t)}{dt} = R_{27}(z,t)N_2(z,t) - t_7^{-1}N_7(z,t)$$
(4.8)

$$\frac{dN_6(z,t)}{dt} = -t_6^{-1}N_6(z,t) + \beta_{76}\tau^{-1}N_7(z,t)$$
(4.9)

$$\frac{dN_5(z,t)}{dt} = R_{15}(z,t)N_1(z,t) - \tau_5^{-1}N_5(z,t) + \sum_{i=6,7} \left[\beta_{i5}\tau_i^{-1}N_i(z,t)\right] - SE_{51} - SE_{50}$$

(4.10)

$$\frac{dN_4(z,t)}{dt} = \sum_{i=5,7} \left[\beta_{i4} \tau_i^{-1} N_i(z,t) \right] - t_4^{-1} N_4(z,t)$$
(4.11)

$$\frac{dN_3(z,t)}{dt} = \sum_{i=4,7} \left[\beta_{i3} \tau_i^{-1} N_i(z,t) \right] - t_3^{-1} N_3(z,t) + R_{03}(z,t) N_0(z,t)$$
(4.12)

$$\frac{dN_2(z,t)}{dt} = \sum_{i=3..7} \left[\beta_{i2} \tau_i^{-1} N_i(z,t) \right] - t_2^{-1} N_2(z,t) - R_{27}(z,t) N_2(z,t) - SE_{21} - SE_{20}$$

(4.13)

$$\frac{dN_1(z,t)}{dt} = -R_{15}(z,t)N_1(z,t) - \sum_{i=2..7} \left[\beta_{i1}\tau_i^{-1}N_i(z,t)\right] + SE_{10} + SE_{20} + SE_{50} \quad (4.14)$$

$$N_0(z,t) = N_{Er} - \sum_{i=1}^{7} N_i(z,t)$$
(4.15)

where N_i is the ith energy level, SE_{ij} is stimulated emission between energy levels N_i and N_j , and R_{ij} is stimulated absorption from energy level N_i to N_j .

Branching Ratios

$\beta_{10} = 1.00$	$\beta_{54} = 0.306$
$\beta_{21} = 0.370$	$\beta_{51} = 0.179$
$\beta_{20} = 0.630$	$\beta_{50} = 0.515$
$\beta_{32} = 1.00$	$\beta_{65} = 0.941$
$\beta_{43} = 0.85$	$\beta_{60} = 0.059$
$\beta_{40} = 0.15$	$\beta_{76} = 1.00$

intrinsic times

$\tau_1 = 9 \text{ ms}$	$ au_2 = 6.7 \text{ ms}$
$\tau_3 = 6.6 \ \mu s$	$\tau_4 = 100 \; \mu \mathrm{s}$
$\tau_5 = 400 \; \mu \mathrm{s}$	$\tau_6 = 5 \ \mu \mathrm{s}$
$\tau_7 = 5 \ \mu \mathrm{s}$	

Once steady state is reached, and all the population levels remain static, the time step is concluded and the new signal and pump powers can be found by using the steady state values for population densities N

$$P_{Signal}(z+1) = P_{Signal}(z) + dz(0.07\epsilon_{Spont} + R_{SE} + \alpha_S P_{Signal}(z))$$
(4.16)

$$P_{Pump}(z+1) = P_{Pump}(z) + dz(\alpha(z)\Gamma_P P_{Pump}(z) + \alpha_P P_{Pump}(z))$$
(4.17)

where $\alpha(z) = \sum_{i=1}^{n} \sigma_{i} N_{i}(z)$, N_{i} is the population density of the energy level $i\left(\frac{Ions}{m^{3}}\right) \sigma_{i}$ is the absorption cross-section (m^{2}) , ϵ_{Spont} is the spontaneous emission factor feeding the light into the signal: $\epsilon_{Spont} = (1-e^{-1})N_{2}(z)\beta_{21}r_{core}^{2}\pi\lambda_{S}^{-1}\frac{hc}{\tau_{2}}\gamma_{21}\left(\frac{W}{m}\right)$ where the β_{21} is the branching ratio from $N_{2} \rightarrow N_{1}$ and γ_{21} is the corresponding spontaneous emission radiative fraction of the $N_{2} \rightarrow N_{1}$ transition, and τ is the intrinsic lifetime of the energy level. 0.07 is the fraction of solid angle that gets guided in a fiber of NA = 0.21. α_{S} and α_{P} are the material losses at the signal and pump wavelengths respectively. Γ_{P} is the pump power filling factor. Once the signal reaches the end of the fiber, it is sent back with a reflectivity of 0.04% to represent Fresnel reflections. The output after each round trip is recorded and the simulation ends when the difference between two consecutive output powers reaches a 0.001% change.

4.2 Simulation Results

First, the absorption of the pump is measured experimentally by pumping a 25 cm length of fiber and measuring the output power. Due to such a short fiber length, there is very little generation of other wavelengths, and hence most of the output power is the residual pump. Figure 4.4, shows the results of the experiment in black and the simulated absorption for a fiber of the same length in blue.

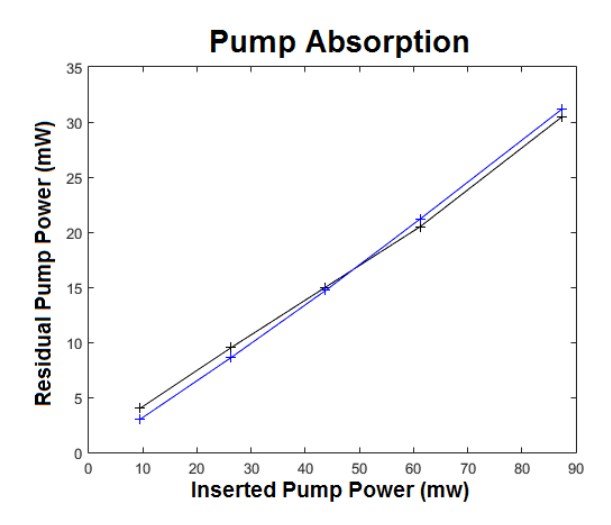
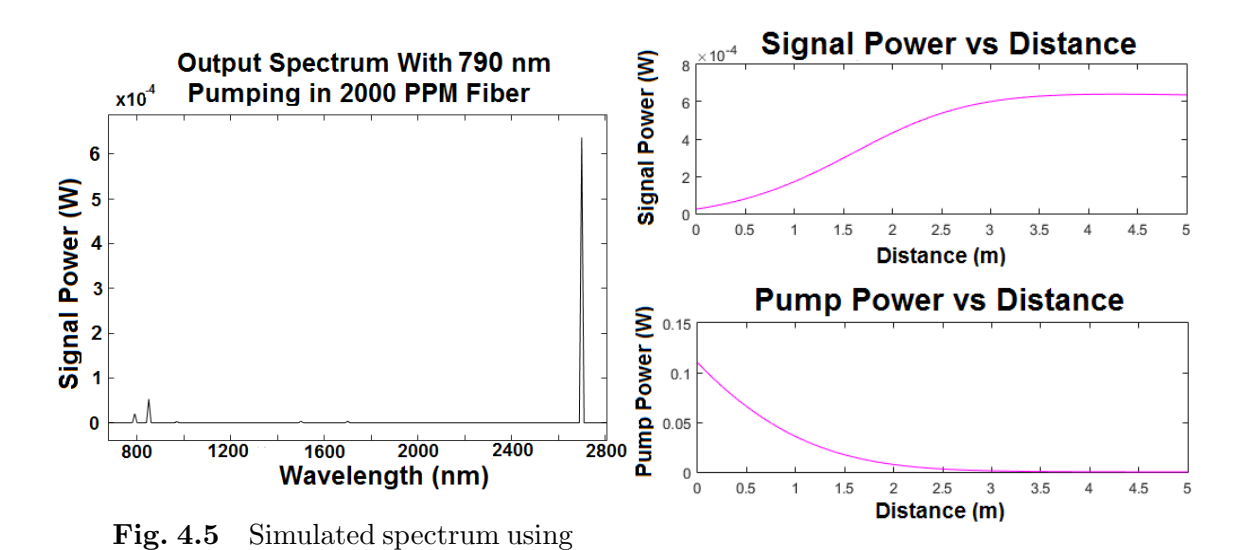


Fig. 4.4 The experimental/simulated 790 nm wavelength absorption through 25 cm of 2000 ppm fiber (black/blue).

The simulation and experiment match closely, however the simulated residual pump has a higher slope than that of the experiment and as such is a worse approximation for higher pump powers. However, since the two match so closely, the laser model parameters used in the simulations seem valid.

4.2.1 Pumping a 2000 ppm Er:ZBLAN Fiber With A 790 nm Wavelength



790 nm wavelength with the 2000

ppm fiber.

Fig. 4.6

distance.

2700 nm signal power and

790 nm pump power as a function of

The simulated spectrum in figure 4.5 resembles closely the experimental counterpart figure 3.5; the only two relevant signals other than the dominant 2700 nm, are the 850 nm and residual 790 nm spectral powers. However, more quantitatively, the ratio between the residual 790 nm power and generated 2700 nm power is 30 as opposed to 50 in the experimental case. Further, the total output power is lower in the simulated case with a total of 4 mW (3.5 mW from 550 nm not shown in figure 4.5) as opposed to 13 mW in experiment. The total output signal power from figure 4.6 is 600 μ W, which is much higher than what was measured of 250 μ W in experiment, although recall the experimental measurement had a large uncertainty due to beam divergence and optical path length related to the filter placement. From the total output power discrepancy, it can be concluded that the model underestimates the spontaneous emission from the green (550 nm) transition, and perhaps the green transition experiences stimulated emission in some sections of the fiber due to ground state bleaching. However, no data is found on the absorption and emission cross sections of the 550 nm transition, and thus this remains a flaw of this erbium model. Figure 4.7 depicts relevant population levels $(N_1, N_2, N_5, \text{ and } N_0)$ at different points of the fiber to give an idea of population inversion levels. Notice that N_2 and N_5 respectively, are twice and equally as populated as the ground state N_0 at the beginning of the fiber. This reveals ground state bleaching. Furthermore, N_2 is higher than N_1 for most of the fiber length, however the 2.7 $\mu \mathrm{m}$ gain tapers off around 4 m from figure 4.6, and thus the optimal length with Fresnel reflections is predicted to be 4 m.

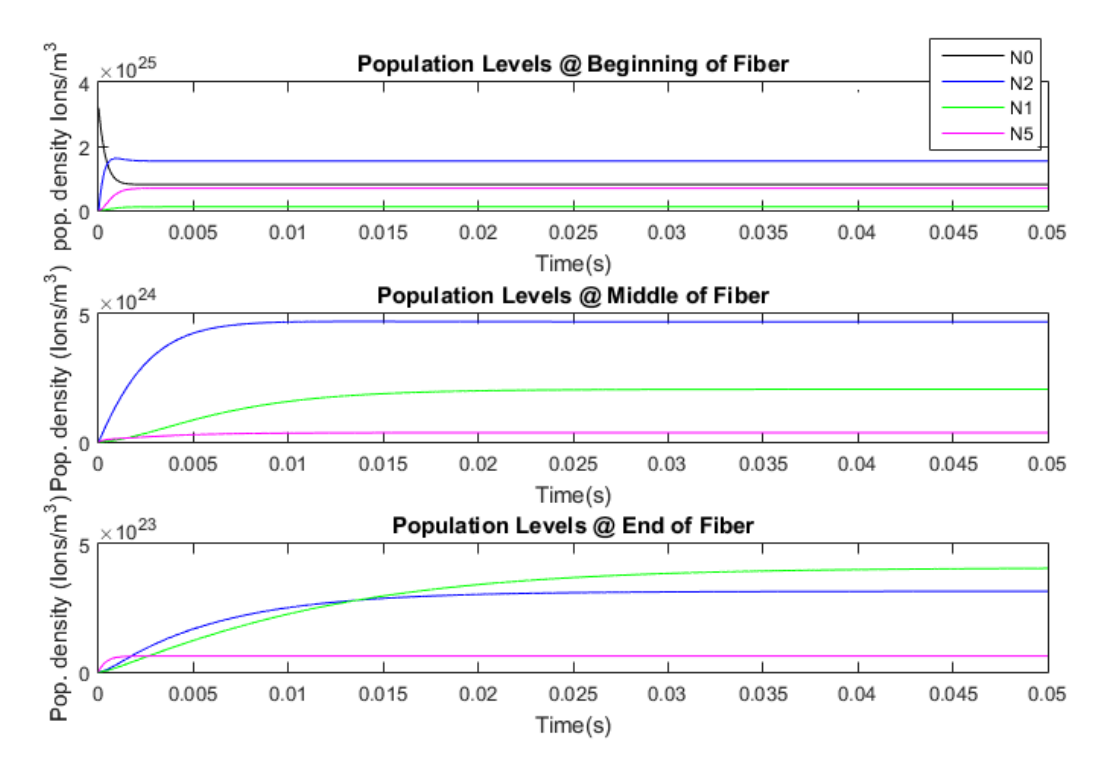
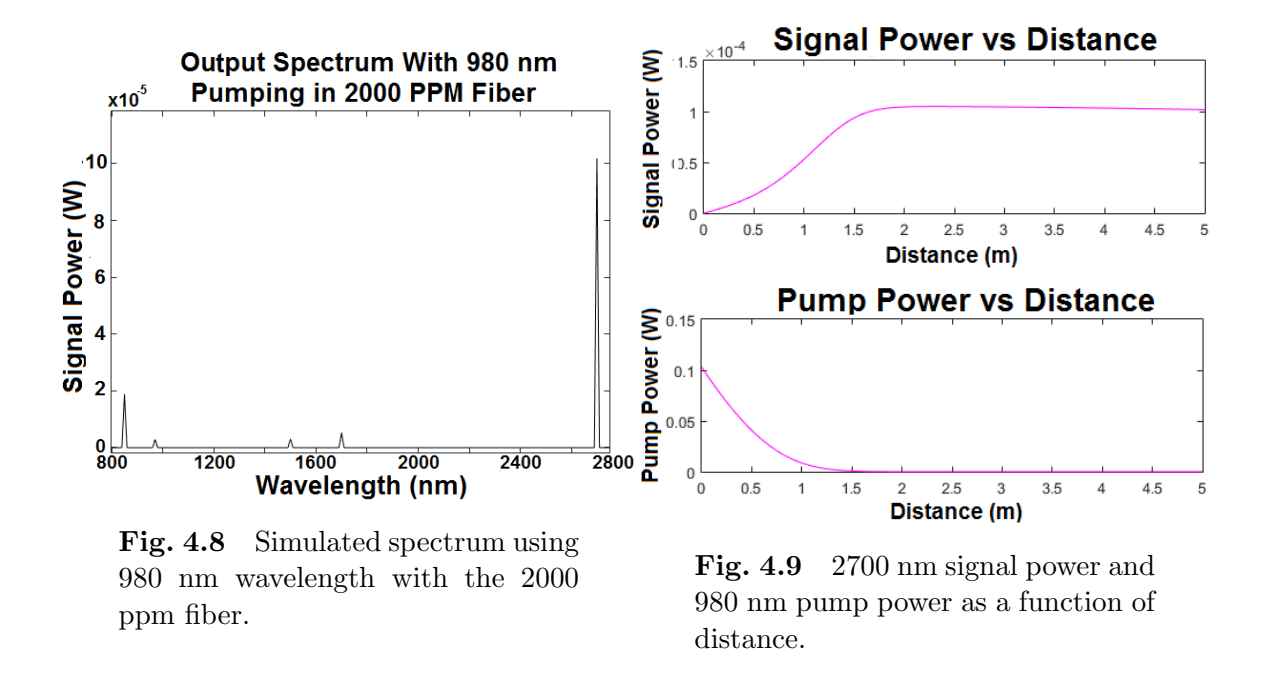


Fig. 4.7 Population densities of important population levels at the beginning middle and end of the fiber for a 2000 PPM Er:ZBLAN fiber pumped at a wavelength of 790 nm.

4.2.2 Pumping a 2000 ppm Er:ZBLAN Fiber With a 980 nm Wavelength

The simulated spectrum in figure 4.8 matches well with the corresponding figure 3.4. Specifically, there is strong evidence of spectral power for the wavelengths of 1700 nm and 850 nm, and the total output power at the wavelength of 2700 nm is 100 μ W . The 100 μ W spectral power at 2700 nm could match close to the 60 μ W measured in experiment when considering the measurement uncertainty. Similarly, the total output power is less than what is realized in experiment at 1 mW total compared to 6 mW in simulation and experiment respectively, due to the same stimulated emission modeling problem concerning the strong 550 nm transition in the presence of ground state bleaching. Another interesting aspect to note is the quick absorption of the 980 nm wavelength in comparison to the 790 nm wavelength. The 980 nm pump power



is almost completely absorbed at 1.5 m from figure 4.9, and 3 m for 790 nm pump.

This quick absorption is an issue because as evidenced in the population levels (figure 4.10), the ESA from the upper laser level (N_2) causes the beginning of the fiber to not have population inversion with respect to the N_1 level with the N_5 level consequently taking precedence. As a result, the population inversion is weak throughout the fiber, and the 2700 nm signal saturates at about 1.75 m. Thus 1.75 m is predicted to be the optimum length after which the 2.7 μ m signal can be absorbed. The point where the pump is mostly absorbed can be roughly seen experimentally by where the green fluorescence disappears. Shown in figures 4.11 and 4.12 are the result of pumping by a weak 790 nm signal and strong 980 nm signal into a 3 m fiber. Notice the fluorescence only lasts about half way (1.5 m) in the 980 nm case and the entire 3 m for the 790 case. This validates the simulation results.

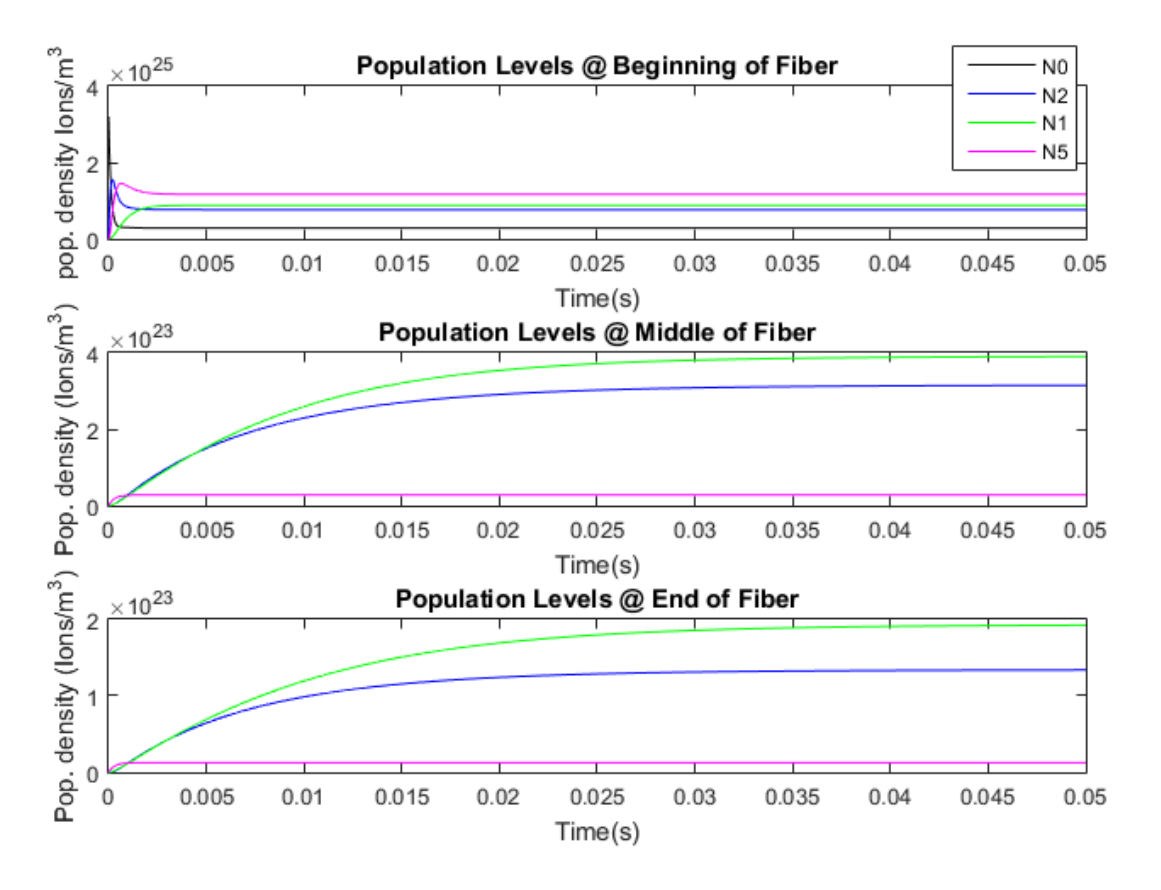


Fig. 4.10 Population densities of important population levels at the beginning middle and end of the fiber for a 2000 PPM Er:ZBLAN fiber pumped at a wavelength of 980 nm.



Fig. 4.11 790 nm wavelength pumping. Notice how the weak free-space coupled 790 nm signal remains strong enough to fluoresce at 550 nm at the end of a 3 m length fiber.

Fig. 4.12 980 nm wavelength pumping. Notice how the strong direct-coupled 980 nm signal is no longer strong enough to fluoresce after about 1.5 m traveled in the fiber

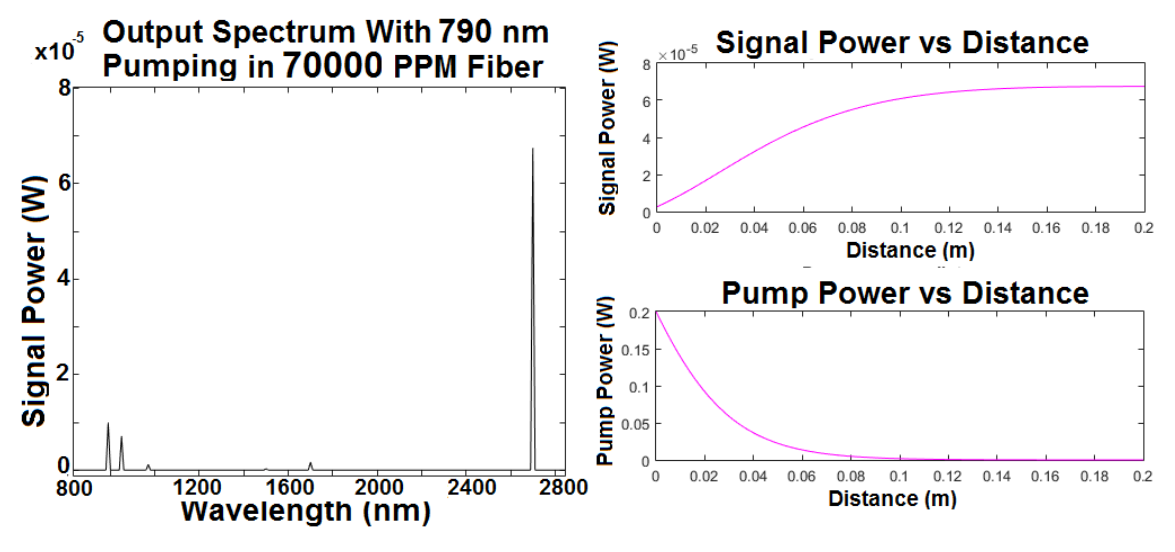


Fig. 4.13 Simulated spectrum using 790 nm wavelength with the 70000 ppm fiber.

Fig. 4.14 2700 nm signal power and 790 nm pump power as a function of distance.

4.2.3 Predicted Performance of a 70000 PPM Fiber

The 70000 ppm ZBLAN laser is simulated over a much smaller stretch of fiber, 20 cm relative to the 5 m for the 2000 ppm fiber. The output spectrum in figure 4.13 shows about 70 μ W of power at the wavelength of 2700 nm as well as a signal at 850 nm along with a very small peak at 1700 nm. The 2700 nm signal power is not converted as efficiently as in the 2000 ppm case, as seen by 200 mW of pump only being converted to 70 μ W while the 100 mW of pump is converted to 600 μ W in the 2000 ppm case. This lack of efficiency is due to a much larger pump absorption occurring due to the increased population density of the ground state N_0 , and thus while there is a much larger population inversion early on in the fiber, the rapid pump absorption does not allow the population inversion to be strongly maintained. As such, the 2700 nm signal gain plateaus around a 20 cm length, not having received a strong overall gain. However, despite the reduced output power at the 2700 nm wavelength, this fiber shows promise in that it sufficiently absorbs most of the 790 nm pump in a very short 20 cm segment of the fiber. Due to this advantage, and the fact that this fiber is much more viable for free-space coupling, recall that 200 mW of

launched power was required to attain 100 mW inserted power in the 2000 ppm case, the 70000 ppm fiber has much more potential for real world applications compared to the 2000 ppm fiber.

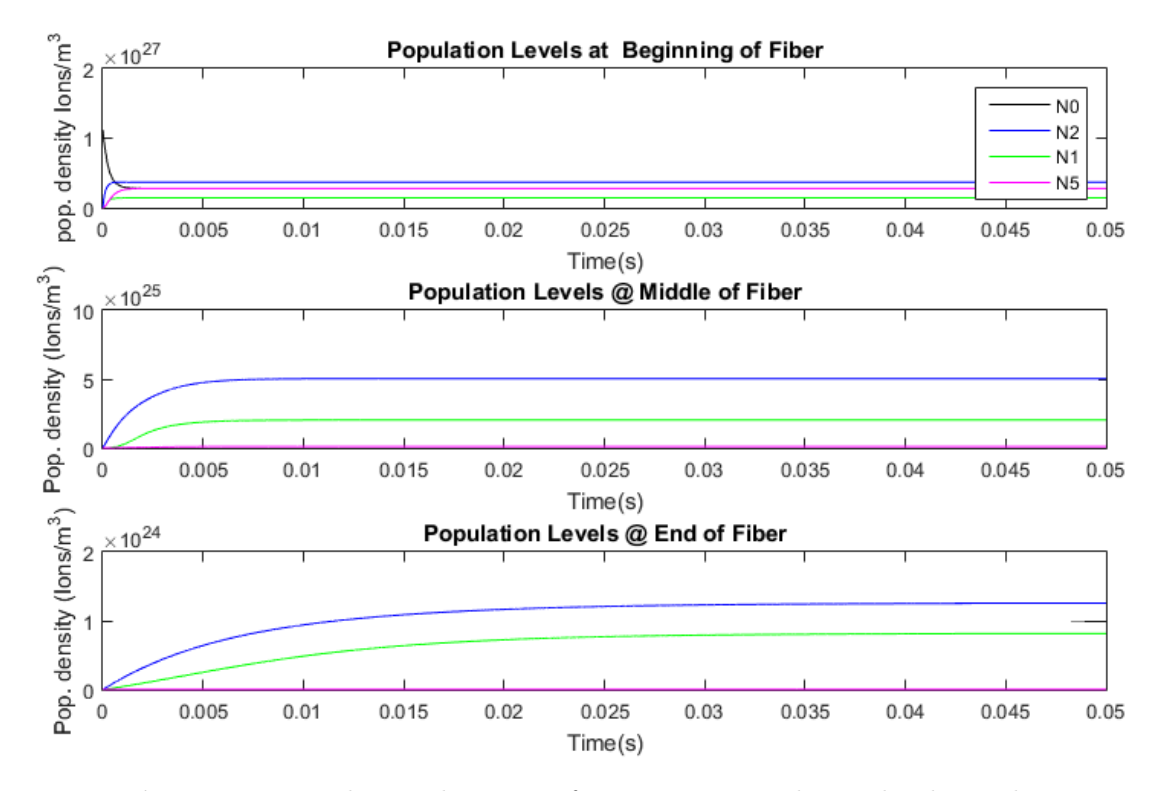


Fig. 4.15 Population densities of important population levels at the beginning middle and end of the fiber for a 70000 PPM Er:ZBLAN fiber pumped at a wavelength of 790 nm.

Notice that the two possible ESA's from the lower laser level and upper laser level are not significant at high doping and low pumping power. Further, since the concentration of erbium is high, the ETU's from both of those levels will become dominant over the ESA's, contrary to the low concentration 2000 ppm case. As such, the 790 nm wavelength pumping is very similar to the 980 nm wavelength energy level regime, except that the pump feeds the N_3 level rather than directly the upper laser level. This result may mean that in highly doped erbium ZBLAN fibers, the 790 nm wavelength could benefit from the energy recycling ETU processes in the same way as the 980 nm wavelength regime is known for.

Evidence of the ETU processes as well as lack of ESA's is seen from figure 4.15.

Notice that the N_5 population level is only relevant at the beginning of the fiber and becomes insignificant at the middle and end. This is the result of GSA dominating the other absorptions. Population inversion between N_2 and N_1 is maintained throughout the fiber however becomes significantly weaker near the end.

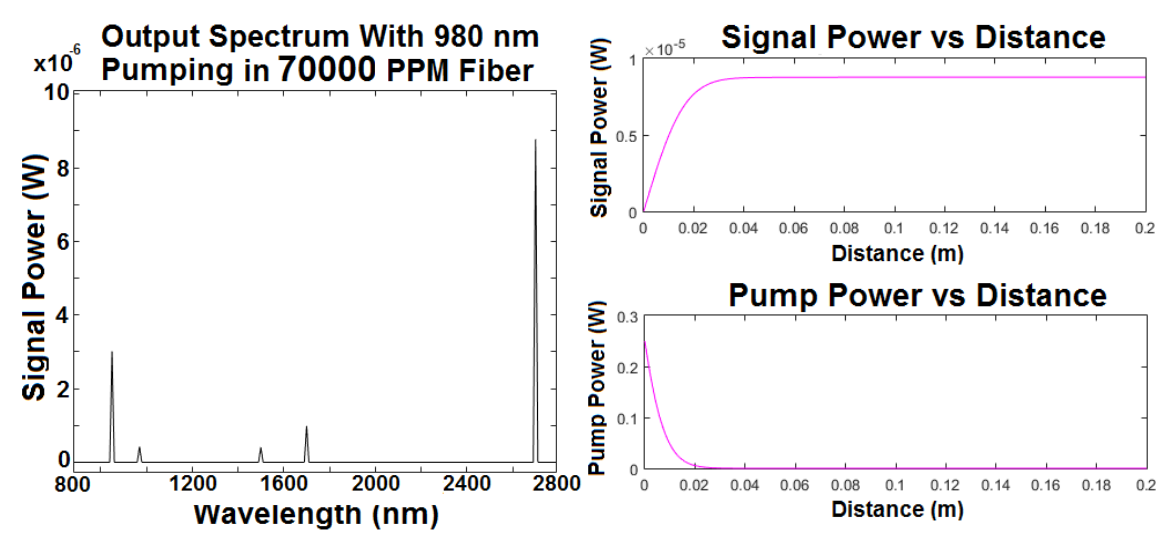


Fig. 4.16 Simulated spectrum using 980 nm wavelength with the 70000 ppm fiber.

Fig. 4.17 2700 nm signal power and 980 nm pump power as a function of distance.

Figure 4.16 shows the predicted output spectrum through 20 cm of 70000 ppm doped fiber. There is a strong excitement of 850 nm and 1700 nm wavelengths and the 2700 nm output power only around 10 μ W. The power is absorbed much quicker than in the 790 nm case and as such after 2 cm is effectively depleted. The optimum distance from figure 4.17 is about 3 cm. The quick absorption is an issue here because the simulation assumes core pumping, which is what is done experimentally with our constraint of low power. However, core pumping can reduce the pump filling factor Γ_P in equation 4.17 to 0.09 which drastically reduces the pump absorption allowing the pump power to be used more efficiently [12]. Figure 4.18 shows the population levels are well inverted at the beginning of the fiber, but as the pump is quickly absorbed over the first few centimeters the population inversion becomes unfavorable.

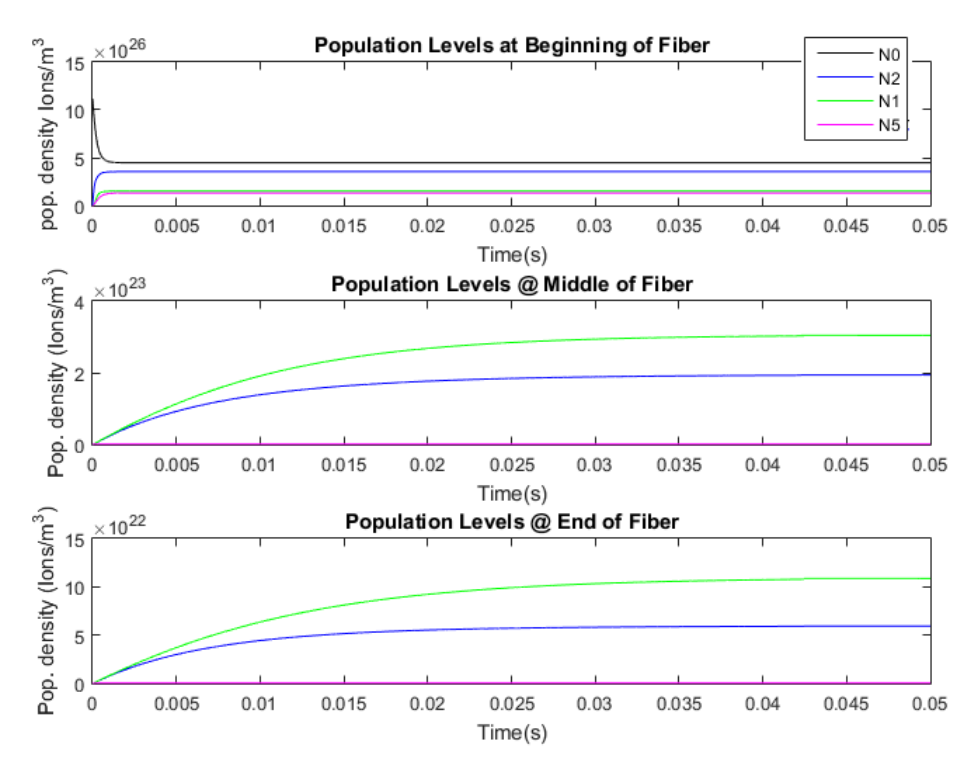


Fig. 4.18 Population densities of important population levels at the beginning middle and end of the fiber for a 70000 PPM Er:ZBLAN fiber pumped at a wavelength of 980 nm.

4.3 Summary of Results

Due to the high erbium concentration causing most pump absorption to happen from the ground state and increased ETU processes which are N^2 dependent, for both the 790 nm and 980 nm pumping wavelengths, both may benefit from population inversion aiding energy recycling. Further, the 790 nm wavelength pump, which has been shown to have greater gain at 2700 nm from experiments, may not be impaired by excitation of the lower laser level filling 850 nm transition which is known to saturate its output at lower erbium concentrations. This is because the upper level of the 850 nm wavelength transition is N_5 is a result of ESA's that occur less frequently in high doping. Moreover, in high power laser designs, it has been predicted in [12] that maximum output power at 2700 nm is saturated using the 980 nm wavelength pump due to the onset of ESA from the upper laser level. A 790 nm pumping wavelength could solve this issue at very high powers because of the favorable ESA from the lower

laser level compared to the upper. Thus the 790 nm pump with the 70000 ppm fiber shows good promise for both low and high power 2700 nm wavelength laser designs.

Conclusion

An Er³⁺ doped ZBLAN fluorescent source was built and studied with respect to the output spectrum through pumping by both 790 nm and 980 wavelengths. The results demonstrated the 790 nm wavelength pumping has favorable performance with respect to the 980 nm wavelength for low power pumping. Specifically, the gain at the wavelength of 2.7 μ m was much better with 790 nm pump. However, due to the ZBLAN fiber dimensions, advancing the project and making a free-space coupled linear laser cavity was deemed impractical at low pump powers due to high losses in the proposed design. Subsequently, a new fiber design was proposed solving the loss issue and opening the possibility for a more compact design. Using results from the fluorescence experiment, and erbium rate equations, a numerical model was made and the proposed fiber was tested numerically. The simulations confirmed that 790 nm is a superior pump in terms of output power at 2.7 μ m, and that the optimum length of the new heavily doped erbium fiber is about 20 cm. Future work on this project aims at building a CW laser based on the results of this thesis, and further to build a compact pulsed 2.7 μ m source.

References

- [1] "NASA Earth Observatory: Home". Earthobservatory.nasa.gov. N.p., 2016. Web. 12 Dec. (2016).
- [2] M. Pollnau, and S. Jackson, "Erbium 3 μ m fiber lasers," IEEE journal on selected topics in quantum electronics, vol. 7, NO. 1 (2001).
- [3] W. Petrich, "Mid-Infrared and raman spectroscopy for medical diagnostics," Applied Spectroscopy Reviews 36.2-3, pp. 181-237 (2001).
- [4] H.Chui, "Mid-infrared light generation by nonlinear optical frequency generation," Stanford Press (1994).
- [5] G. Agrawal, "Nonlinear fiber optics fifth edition," Academic Press (2013).
- [6] X. Zhu, and R.Jain, "10-W-level diode-pumped compact 2.78 μm ZBLAN fiber laser." Opt. Lett. 32, pp. 26 - 28 (2007).
- [7] S. Tokita, M. Murakami, S. Shimizu, M. Hashida, and S. Sakabe, "12 W Q-switched Er:ZBLAN fiber laser at 2.8 μ m," Opt. Lett. 36, pp. 2812 2814 (2011).
- [8] O. Henderson-Sapir, S. D. Jackson, and D. J. Ottaway, "Versatile and widely tunablemid-infrared erbium doped ZBLAN fiber laser," Opt. Lett., vol. 41, no. 7, pp. 1676 – 1679, Apr (2016).

References 58

[9] C. Berge, A. Al Kadry, and M. Rochette "Comparison of 2.7 micron fluorescent spectra of er-zblan with 980 nm and 790 nm pumping," at Photonics North, Highpower-4-29-6, Ottawa, Ontario (2015).

- [10] V. Ter-Mikirtychev, "Fundamentals of fiber lasers and fiber amplifiers," 1st ed. Switzerland: Springer International Publishing, (2014).
- [11] T. Okoshi, "Optical fibers," 1st ed. New York: Academic Press, (1982).
- [12] J. Li, S. D. Jackson, "Numerical modeling and optimization of diode pumped heavily-erbium-doped fluoride fiber lasers," IEEE J. Quant. Electron. 48, pp. 454-464 (2012).
- [13] S. Murray, M.O Scully, and W. E Lamb, "Laser physics," 1st ed. Reading, Mass.: Addison-Wesley Pub. Co., Advanced Book Program, (1974).
- [14] G. Liu, "K. Advances in the theoretical understanding of photon upconversion in rare-earth activated nanophosphors," Chemistry Social Review, vol. 44, no. 6, pp. 1635-1652 (2015).
- [15] M. Pollnau, R. Spring, Ch. Ghisler, S.Wittwer, W. Luthy, and H. P. Weber, "Efficiency of erbium 3-μm crystal and fiber lasers," IEEE Journal of Quantum Electronics, vol. 32, no. 4, pp. 657-663 (1996).
- [16] M. Pollnau, Ch. Ghisler, G. Bunea, M. Bunea, W. Lthy, and H.P. Weber, "150 mW unsaturated output power at 3 μ m from a single-mode-fiber erbium cascade laser," Applied Physics Letters, 66 (26). pp. 3564-3566 (1995).
- [17] M. Pollnau, S. Bedo, w. Luthy, H.P and Weber, "On the saturation of the 791 nm pumped erbium 3 μ m fiber laser." Tech. Dig. Conf. Advanced Solid-State Lasers, Memphis, Tennessee, (1995).

References 59

[18] V. Fortin, F. Maes, M. Bernier, S. Toubou Bah, M. D
Auteuil, and R. Vallée, "Watt-level erbium-doped all-fiber laser at 3.44
 $\mu \rm m$," Opt. Lett. 41, pp. 559-562 (2016)

- [19] V. Fortin, F. Maes, M. Bernier, S. Toubou Bah, M. DAuteuil, and R. Vallée, "30W Fluoride Glass All-Fiber Laser At 2.94 μ m," Optics Letters 40.12 (2015).
- [20] M. Pollnau and S. D. Jackson, "Energy recycling versus lifetime quenching in erbium-doped 3- μ m fiber lasers," IEEE Journal of Quantum Electronics, vol. 38, no. 2, pp. 162-169 (2002).
- [21] C.R. Pol lock, and M. Lipson, "Integrated photonics," 1st ed. Boston: Kluwer Academic (2003).

Appendix

Pumping Er:ZBLAN With 790 nm Code

```
%Cameron Berge - Cameron.berge@mail.mcgill.ca
%260483464
%%% ER:ZBLAN simulations for 790 nm pumping
% inspired by references [1][2][3]
\% Not included other stimulated emissions other than 2.7 um
%-----PARAMETERS AND DEFINITIONS-----
%
%GammaS = Signal overlap factor
%GammaP = pump overlap factor
%----- Crossections (m^2) -----
% SigmaES = Signals stimulated emission crossection
% SigmaAS = signals absorption crossection
% SigmaEP = pump stimulated emission crossection
% SignamAP = pump stimulated absorption crossection
% ----- Energy Levels (Ions/m^3)-----
% N7 = ESA2 Level
```

```
% N6 = High energy level
% N5 = ESA1 level
% N4 = intermediate level
% N3 = ground state pump absorption level
% N2 = upper level Ion population density
% N1 = lower level Ion population density
% NO = Ground state
%----- Fiber Parameters -----
% Nt = total ion population Ions/m<sup>3</sup>
% L = length of the fiber (m)
% Nsub = number of subdivisions of the fiber
%A = fiber core area m^2
%----- Pump Parameters -----
% Pp = Pump power (W)
% LambdaP = pump wavelength (m)
%-----
% Ps = signal power (W)
% vs = signal frequency (Hz)
% vp = pump frequency (Hz)
% tsp = spontaneos emission lifetime (s)
\% h = plancks constant 6.62606957 ? 10-34 m2 kg / s
% g = signal gain at point z
% a = signal attenuation at point z
% LambdaS = signal wavelength
%-----
%constant parameters
```

```
h = 6.62606957e-34;
c = 3e8;
LambdaS = 2700e-9;
LambdaP = 790e-9;
RoundTrips = 5;
%-----INTRINSIC LIFE TIMES-----
%(s)
t1 = 9e-3; t2 = 6.9e-3; t3 = 10e-6; t4 = 120e-6;
t5 = 570e-6; t6 = 5e-6; t7 = 5e-6;
%----- BRANCHING RATIOS-----
B10 = 1.00; B54 = 0.306;
B21 = 0.370; B51 = 0.179;
B20 = 0.630;
            B50 = 0.515;
B32 = 1.00; B65 = 0.941;
B43 = 0.85; B60 = 0.059;
B40 = 0.15; B76 = 1.00;
%-----CROSSECTIONS-----
\%(m^2)
sigma03 = 7e-26; sigma15 = 1.2e-25; sigma27 = .5e-27;
sigma21 = 4.2e-25;
%Input parameters
Time = 0.10; % 1 second
L = .2; %length of the Er:ZBLAN fiber (m)
Nsub = 100; % Spatial Subdivisions (need to vary if changing length of fiber)
Tsub = 5000; %Temporal Subdivisions
%GammaP = .0057; %double clad
```

```
GammaP = .9; % ratio of core area to double clad area aprox. 1 if core pumped
GammaS = .91;
Ppo790 = 20;
%Nt = 3.2e25; %Erbium Concentration Atoms/m^3 %3.2e25 is approx. 2000 ppm Er
Nt = 9.6e26;
rcore = 12.5e-6; %Core radius (m)
pi = 3.1415926;
Rp1 = 0.04; % Pump reflectivity at input
Rp2 = 0.04;  % Pump reflectivity at output
Rs1 = .998; % Signal reflectivity at input
Rs2 = 0.04; % output end 0.04 is fresnel reflections
z = 0 : L/Nsub : L; % fiber length array with subdivisions
% Degeneracy
g1 = 2;
g2 = 2;
%Boltzmann
b1 = 0.113;
b2 = 0.200;
% b1 = 0.096;
\% b2 = 0.16;
% Population vectors of each energy level
t = 0 : Time/Tsub : Time;
RSE21 = zeros(Tsub, Nsub);
% AeffS = 240.8e-12;
% AeffP = 117e-12;
```

```
AeffP = 3.14*1e-10;
AeffS = 3.14*1e-10;
PumpBack = zeros(Nsub,1);
signalBack = zeros(Nsub,1);
signalForw= zeros(Nsub,1);
RGSA = zeros(Tsub,Nsub);
RESA = zeros(Tsub,Nsub);
alphaeff = zeros(Tsub,Nsub);
% Initial Photon density
%Phi52(1,1) = 0; 1.7 \text{ um transition}
PumpForw = zeros(1,Nsub);
PumpForw(1) = Ppo790;
PumpForw(1) = Ppo790;
OutPut = zeros(RoundTrips,1);
%Phi21 calculation
Ntest = zeros(10,1);
% Input Parameters
dt = Time/Tsub;
dz = L/Nsub;
```

```
%Independent and Dependent variables
alpha = zeros(1,Nsub);
%Gain in the slices
Signal(1) = 0;
Signal53(1) = 0;
Signal51(1) = 0;
Signal50(1) = 0;
Signal20(1) = 0;
Signal10(1) = 0;
% for f = 1:Nsub
%
      PumpBackward(f+1) = PumpBackward(f)*2;
% end
% W11 = 3.6e-23;
% W22 = 1.2e-23;
% W50 = 2.7e-23;
W11 = 1e-24;
W22 = .3e-24;
W50 = .5e-24;
NO = zeros(Tsub, Nsub);
N1 = zeros(Tsub, Nsub);
N2 = zeros(Tsub, Nsub);
N3 = zeros(Tsub, Nsub);
N4 = zeros(Tsub, Nsub);
N5 = zeros(Tsub,Nsub);
```

```
N6 = zeros(Tsub, Nsub);
N7 = zeros(Tsub, Nsub);
for Q = 1:RoundTrips % this is the number of cycles
% Signal(1) = Pso*Q;
if Q >1
%
     if mod(Q,2) == 1
%
     PumpForw(1) = Ppo980;
%
     else
%
        PumpBack(1) = PumpForw(1)*R;
%
     end
end
PumpForw;
for i=1:(Nsub)
for j=1:Tsub
% pumpinfo790 = (LambdaP/(h*c*pi*rcore^2))*(pumpBack(i)+ pumpForw(i));
%
   else
pumpinfo790 = (LambdaP/(h*c*AeffP))*(PumpForw(i) + PumpBack(i));
%
      SE21(j+1,i) = (b2*N2(i)-(g2/g1)*b1*N1(i))*sigma21*c*Phi21(j,i); % 2.7 um
%
      SE10(j+1,i) = (b1*N1(i)-(g1/g2)*b0*N0(i))*sigma15*c*Phi21(j,i); % 1.5 um
%
      SE20(j+1,i) = (b2*N2(i)-(g2/g1)*b1*N0(i))*sigma21*c*Phi20(j,i); % 980 nm
%
      SE51(j+1,i) = (b2*N2(i)-(g5/g1)*b1*N1(i))*sigma15*c*Phi51(j,i); % 850 nm
%
      SE50(j+1,i) = (b2*N2(i)-(g5/g0)*b0*N0(i))*sigma15*c*Phi50(j,i); % 550 nm
% signal53info = (1700e-9)/(h*c*pi*rcore^2);
\% signal51info = (850e-9)/(h*c*pi*rcore^2);
```

```
% signal50info = (550e-9)/(h*c*pi*rcore^2);
% signal10info = (1500e-9)/(h*c*pi*rcore^2);
% signal20info = (970e-9)/(h*c*pi*rcore^2);
%
     if mod(RoundTrips,2) == 0
% pumpinfo790 = (LambdaP/(h*c*pi*rcore^2))*PumpBackward(i);
%
%
    else
% pumpinfo790 = (LambdaP/(h*c*pi*rcore^2))*Pp790(i);
%
     end
signalinfo = (LambdaS*GammaS/(h*c*AeffS )); %2.7
%980 pump absorptions
%790 pump absorptions
%
%
       RESA = N2(j,i)*sigma27*(sigma03*N0(j,i)+sigma15*N1(j,i)
%+sigma27*N2(j,i))^-1*...
              (1-\exp(-(sigma03*N0(j,i)+sigma15*N1(j,i)+sigma27*N2(j,i))*dz))
%
%*pumpinfo790;
%
              %
                     R15 = N1(j,i)*sigma15*(sigma03*N0(j,i)+sigma15*N1(j,i))
%+sigma27*N2(j,i))^-1*...
%
              (1-\exp(-(sigma03*N0(j,i)+sigma15*N1(j,i)+sigma27*N2(j,i))*dz)
%)*pumpinfo790;
                     RGSA= NO(j,i)*sigma03*(sigma03*NO(j,i)+sigma15*N1(j,i)
%
              %
%+sigma27*N2(j,i))^-1*...
%
              (1-\exp(-(sigma03*N0(j,i)+sigma15*N1(j,i)+sigma27*N2(j,i))*dz)
%)*pumpinfo790;
%
```

```
%
              %
                     RESA = N2(j,i)*sigma26*(sigma02*N0(j,i)+sigma26*N2(j,i)
%))^-1*...
%
              (1-\exp(-((sigma02*N0(j,i)+sigma26*N2(j,i))*dz)))*pumpinfo980;
%
       RGSA= NO(j,i)*sigma02*(sigma02*NO(j,i)+sigma26*N1(j,i))
%^-1...
%*(1-\exp(-(sigma02*NO(j,i)+sigma26*N2(j,i))*dz))*pumpinfo980;
RESA = N2(j,i)*sigma27*pumpinfo790*GammaP;
RGSA= NO(j,i)*sigma03*pumpinfo790*GammaP;
R15 = N1(j,i)*sigma15*pumpinfo790*GammaP;
% Possible Stimulated Emissions
RSE21 = (b2*N2(j,i)-(g2/g1)*b1*N1(j,i))*sigma21*...
(signalForw(i)+signalBack(i)); % LASING AT 2.7 um
k1N7 = (-N7(j,i)/t7 + RESA);
k1N6 = (-N6(j,i)/t6 + N7(j,i)/t7 + W22*N2(j,i).^2);
k1N5 = (-N5(j,i)/t5 + N6(j,i)/t6 + R15 - W50*N5(j,i)...
.*NO(j,i));
k1N4 = (-N4(j,i)/t4 + B54*1/t5*N5(j,i));
k1N3 = (-N3(j,i)/t3 + B43*1/t4*N4(j,i) + RGSA + W50*N5(j,i)...
.*NO(j,i) + W11.*N1(j,i).^2);
k1N2 = (-N2(j,i)/t2 + B32*1/t3*N3(j,i) - RSE21*signalinfo - RESA...
-2*W22.*N2(j,i).^2);
k1N1 = (-N1(j,i)/t1 + B21*1/t2*N2(j,i) + B51*1/t5*N5(j,i)...
+ RSE21*signalinfo+ - R15 +...
W50.*N5(j,i).*N0(j,i) - 2*W11.*N1(j,i).^2 + W22*N2(j,i).^2);
k2N7 = N7(j,i) + dt/2*k1N7;
```

```
k2N6 = N6(j,i) + dt/2* k1N6;
k2N5 = N5(j,i) + dt/2* k1N5;
k2N4 = N4(j,i) + dt/2* k1N4;
k2N3 = N3(j,i) + dt/2* k1N3;
k2N2 = N2(j,i) + dt/2* k1N2;
k2N1 = N1(j,i) + dt/2* k1N1;
k3N7 = N7(j,i) + dt/2*k2N7;
k3N6 = N6(j,i) + dt/2* k2N6;
k3N5 = N5(j,i) + dt/2* k2N5;
k3N4 = N4(j,i) + dt/2* k2N4;
k3N3 = N3(j,i) + dt/2* k2N3;
k3N2 = N2(j,i) + dt/2* k2N2;
k3N1 = N1(j,i) + dt/2* k2N1;
k4N7 = N7(j,i) + dt*k3N7;
k4N6 = N6(j,i) + dt* k3N6;
k4N5 = N5(j,i) + dt * k3N5;
k4N4 = N4(j,i) + dt* k3N4;
k4N3 = N3(j,i) + dt* k3N3;
k4N2 = N2(j,i) + dt* k3N2;
k4N1 = N1(j,i) + dt* k3N1;
N7(j+1,i) = N7(j,i) + dt/6*(k1N7 + 2*k2N7 + 2*k3N7 + k4N7);
N6(j+1,i) = N6(j,i) + dt/6*(k1N6 + 2*k2N6 + 2*k3N6 + k4N6);
N5(j+1,i) = N5(j,i) + dt/6*(k1N5 + 2*k2N5 + 2*k3N5 + k4N5);
N4(j+1,i) = N4(j,i) + dt/6*(k1N4 + 2*k2N4 + 2*k3N4 + k4N4);
```

```
N3(j+1,i) = N3(j,i) + dt/6*(k1N3 + 2*k2N3 + 2*k3N3 + k4N3);
N2(j+1,i) = N2(j,i) + dt/6*(k1N2 + 2*k2N2 + 2*k3N2 + k4N2);
N1(j+1,i) = N1(j,i) + dt/6*(k1N1 + 2*k2N1 + 2*k3N1 + k4N1);
NO(j+1,i) = Nt - N1(j,i) - N2(j,i) - ...
N3(j,i) - N4(j,i) - N5(j,i) - N6(j,i) - N7(j,i);
if((j<1000))
end
if (Nt < N2(j,i))
break
end
end
%
% Pp(i+1) = Pp(i)*exp(-(sigma03*NO(j,i)+sigma15*N1(j,i)+sigma27*N2(j,i))*dz);
%
%
% Phi21(1,i+1) = Phi21(Tsub,i);
SpontEM2700 = N2(Tsub,i)*B21*rcore^2*pi*(2700e-9)^-1*(h*c)/t2*.318;
% SpontEM1500 = .63*N1(Tsub,i)*B10*rcore^2*pi*(1500e-9)^-1*(h*c)/t1*1e-1;
% SpontEM980 = .63*N2(Tsub,i)*B20*rcore^2*pi*(980e-9)^-1*(h*c)/t2*.3e-1;
% SpontEM850 = .63*N5(Tsub,i)*B51*rcore^2*pi*(850e-9)^-1*(h*c)/t5*.3e-1;
% SpontEM1700 = .63*N1(Tsub,i)*B10*rcore^2*pi*(1500e-9)^-1*(h*c)/t1*.3e-1;
% SpontEM550 = .63*N5(Tsub,i)*B50*rcore^2*pi*(550e-9)^-1*(h*c)/t5;
%
% SpontEM2700 = N2(Tsub,i)*B21*rcore^2*pi*(2700e-9)^-1*(h*c);
% SpontEM1500 = N1(Tsub,i)*B10*rcore^2*pi*(1500e-9)^-1*(h*c);
```

```
% SpontEM980 = N2(Tsub,i)*B20*rcore^2*pi*(980e-9)^-1*(h*c);
% SpontEM850 = N5(Tsub,i)*B51*rcore^2*pi*(850e-9)^-1*(h*c);
% SpontEM1700 = N1(Tsub,i)*B10*rcore^2*pi*(1500e-9)^-1*(h*c);
% SpontEM550 = N5(Tsub,i)*B50*rcore^2*pi*(550e-9)^-1*(h*c);
alpha(i) = sigma03*N0(Tsub,i)+sigma15*N1(Tsub,i)+sigma27*N2(Tsub,i);
if mod(Q,2)==1
PumpForw(i+1) = PumpForw(i)- dz*(alpha(i)*PumpForw(i)*...
GammaP + 3e-3*PumpForw(i));
signalForw(i+1) = (signalForw(i) + dz*(.01*SpontEM2700+ ...
(b2*N2(Tsub,i)-(g2/g1)*b1*N1(Tsub,i))...
*sigma21*GammaS*signalForw(i) -23e-3*signalForw(i)));
else
PumpBack(i+1) = PumpBack(i)- dz*(alpha(i)*PumpBack(i)*GammaP...
+ 3e-3*PumpBack(i));
signalBack(i+1) = (signalBack(i) + dz*(.01*SpontEM2700+...
(b2*N2(Tsub,i)-(g2/g1)*b1*N1(Tsub,i))...
*sigma21*GammaS*signalBack(i) -23e-3*signalBack(i)));
end
end
OutPut(Q) = (1-Rs2)*signalForw(Nsub-1);
if Q>1 && mod(Q,2)==1 && (abs(OutPut(Q) - OutPut(Q-2))/(OutPut(Q))<0.01)
Q
(OutPut(Q) - OutPut(Q-2))/(OutPut(Q))
break
end
```

```
if Q ~= RoundTrips
if mod(Q,2) == 1
signalBack(1) = (Rs2)*signalForw(Nsub);
PumpBack(1) = (Rp2)*PumpForw(Nsub);
PumpForw = PumpForw(end:-1:1);
signalForw = signalForw(end:-1:1);
else
signalForw(1) = (Rs1)*signalBack(Nsub);
PumpForw(1) = (Rp1)*PumpBack(Nsub)+Ppo790;
PumpBack = PumpBack(end:-1:1);
signalBack = signalBack(end:-1:1);
end
else
Signalout = (1-Rs2)*signalForw(Nsub)
end
end
figure,
subplot(3,1,1)
```

```
plot(t,NO(:,1),'k-',t,N2(:,1),'b-', t,N1(:,1),'g-',t,N5(:,1),'m-')
legend('NO', 'N2', 'N1','N5')
title('Population Levels at Beginning of Fiber')
xlabel('Time(s)')
ylabel('pop. density Ions/m^3')
subplot(3,1,2)
plot(t,N2(:,Nsub/2),'b-', t,N1(:,Nsub/2),'g-',t,N5(:,Nsub/2),'m-')
legend('N2', 'N1','N5')
title('Population Levels @ Middle of Fiber')
xlabel('Time(s)')
ylabel('Pop. density (Ions/m^3)')
subplot(3,1,3)
plot(t,N2(:,Nsub),'b-', t,N1(:,Nsub),'g-',t,N5(:,Nsub),'m-')
legend('N2 ', 'N1','N5')
title('Population Levels @ End of Fiber')
xlabel('Time(s)')
ylabel('Pop. density (Ions/m^3)')
figure,
subplot(2,1,1)
plot(z,signalForw,'m-')
legend('Signal')
title('Signal power vs distance')
```

```
xlabel(' Distance (m)')
ylabel('Signal power (W)')
subplot(2,1,2)
plot(z,PumpForw,'m')
title('Pump power vs distance')
xlabel('Distance along fiber (m)
ylabel('Pump Power (W)')
% omega = 500:10:3000;
% siz0 = length(omega);
% dOmeg = 1/10;
% Spectrum = zeros(1,siz0);
% Spectrum(round((850-500)*d0meg)+1)= Signal51(end);
% Spectrum(round((550-500)*d0meg)+1)= Signal50(end);
% Spectrum(round((1500-500)*d0meg)+1)= Signal10(end);
% % Spectrum(round((980-500)*d0meg)+1)= Signal20(end);
% Spectrum(round((1700-500)*d0meg)+1)= Signal53(end);
% Spectrum(round((2700-500)*d0meg)+1)= Signal(end);
% Spectrum(round((980-500)*d0meg)+1)= Pp980(end)+Signal20(end);
% figure,
% plot(omega,Spectrum,'k-')
% [1] M. Pollnau, S. Bedo, w. Luthy, H.P and Weber, ''On the saturation of
```

```
%the 791 nm pumped erbium 3 um fiber laser.'' Tech. Dig. Conf. Advanced Solid-State %Lasers, Memphis, Tennessee, 1993
%[2] M. Pollnau, Ch. Ghisler, G. Bunea, M. Bunea, W. Lthy, and H.P. Weber,
%''150 mW unsaturated output power at 3 $\mu$m from a single-mode-fiber erbium
%cascade laser,'' Applied Physics Letters, 66 (26). pp. 3564-3566, 1995 .
%[3] M. Pollnau and S. D. Jackson, 'Energy recycling versus lifetime
%quenching in erbium-doped 3-$\mu$m fiber
%lasers,'' IEEE Journal of Quantum Electronics, vol. 38, no. 2, pp. 162169, 2003
```

Pumping Er:ZBLAN With 980 nm Code

```
%Cameron Berge - Cameron.berge@mail.mcgill.ca
%260483464
%%% ER:ZBLAN simulations 980 nm pumping
% Not included other stimulated emissions other than 2.7 um
%Inspired by references [1][2][3]
%-----
%-----PARAMETERS AND DEFINITIONS-----
%
%GammaS = Signal overlap factor
%GammaP = pump overlap factor
% SigmaES = Signals stimulated emission crossection
% SigmaAS = signals absorption crossection
% SigmaEP = pump stimulated emission crossection
% SignamAP = pump stimulated absorption crossection
% ----- Energy Levels (Ions/m^3)-----
% N7 = ESA2 Level
```

```
% N6 = High energy level
% N5 = ESA1 level
% N4 = intermediate level
% N3 = ground state pump absorption level
% N2 = upper level Ion population density
% N1 = lower level Ion population density
% NO = Ground state
%----- Fiber Parameters -----
% Nt = total ion population Ions/m<sup>3</sup>
% L = length of the fiber (m)
% Nsub = number of subdivisions of the fiber
%A = fiber core area m^2
%----- Pump Parameters -----
% Pp = Pump power (W)
% LambdaP = pump wavelength (m)
%-----
% Ps = signal power (W)
% vs = signal frequency (Hz)
% vp = pump frequency (Hz)
% tsp = spontaneos emission lifetime (s)
\% h = plancks constant 6.62606957 ? 10-34 m2 kg / s
% g = signal gain at point z
% a = signal attenuation at point z
% LambdaS = signal wavelength
%-----
```

%constant parameters

```
h = 6.62606957e-34;
tsp = 100e-6;
c = 3e8;
LambdaS = 2800e-9;
LambdaP = 976e-9;
vs = c/(LambdaS);
vp = c/(LambdaP);
RoundTrips = 3;
%-----INTRINSIC LIFE TIMES-----
%(S)
t1 = 9e-3; t2 = 6.9e-3; t3 = 10e-6; t4 = 120e-6;
t5 = 570e-6; t6 = 5e-6; t7 = 5e-6; y21 = 0.393;
%----- BRANCHING RATIOS------
B54 = 0.34;
B21 = 0.370; B53 = .006;
B52 = .18; B51 = 0.179;
B65 = 0.941;
B32 = 1.00;
B43 = 0.85;
%-----CROSSECTIONS-----
%(m^2)
sigma21 = 4.2e-25;
sigma26 = 1.1e-25; sigma02 = 2.1e-25;
%Input parameters
Time = 0.25; % 1 second
L = .2; % length of the Er:ZBLAN fiber (m)
Nsub = 100; % Spatial Subdivisions (need to vary if changing length of fiber)
```

```
Tsub = 5000; %Temporal Subdivisions
%GammaP = .0057; %double clad
GammaP = .95; % ratio of core area to double clad area aprox. 1 if multimode core pum
GammaS = .91;
sigmaSE = 5.7e-2;
Ppo980 = 200e-3;
Nt = 3.2e25; %Erbium Concentration Atoms/m<sup>3</sup> 3.2e25 is approx. 2000 ppm Er
%Nt = 9.6e26;
pi = 3.1415926;
Rp1 = 0.04;  % Pump reflectivity at input
Rp2 = 0.04; % Pump reflectivity at output
Rs1 = .998; % Signal reflectivity at input
Rs2 = 0.04; % output end 0.04 is fresnel reflections
z = 0 : L/Nsub : L; % fiber length array with subdivisions
% Degeneracy
g1 = 2;
g2 = 2;
%Boltzmann
b1 = 0.113;
b2 = 0.200;
% b1 = 0.096;
\% b2 = 0.16;
% Population vectors of each energy level
t = 0 : Time/Tsub : Time;
RSE21 = zeros(Tsub, Nsub);
% AeffS = 240.8e-12;
```

```
% AeffP = 117e-12;
AeffP = 3.14*1e-10;
AeffS = 3.14*1e-10;
PumpBack = zeros(Nsub,1);
signalBack = zeros(Nsub,1);
signalForw= zeros(Nsub,1);
RGSA = zeros(Tsub, Nsub);
RESA = zeros(Tsub, Nsub);
PumpForw = zeros(1,Nsub);
PumpForw(1) = Ppo980;
PumpForw(1) = Ppo980;
OutPut = zeros(RoundTrips,1);
% Input Parameters
dt = Time/Tsub;
dz = L/Nsub;
%Independent and Dependent variables
alpha = zeros(1,Nsub);
%Gain in the slices
% for f = 1:Nsub
%
%
      PumpBackward(f+1) = PumpBackward(f)*2;
% end
W11 = 3.6e-23;
W22 = 1.2e-23;
W50 = 2.7e-23;
% W11 = 1e-24;
% W22 = .3e-24;
```

```
% W50 = .5e-24;
NO = zeros(Tsub, Nsub);
N1 = zeros(Tsub, Nsub);
N2 = zeros(Tsub, Nsub);
N3 = zeros(Tsub, Nsub);
N4 = zeros(Tsub, Nsub);
N5 = zeros(Tsub, Nsub);
N6 = zeros(Tsub, Nsub);
N7 = zeros(Tsub, Nsub);
for Q = 1:RoundTrips % this is the number of cycles
% Signal(1) = Pso*Q;
if Q >1
%
     if mod(Q,2) == 1
%
      PumpForw(1) = Ppo980;
%
     else
%
        PumpBack(1) = PumpForw(1)*R;
%
     end
end
PumpForw;
for i=1:(Nsub)
for j=1:Tsub
% converts powers at wavelengths to photons/s*m^2
pumpinfo980 = (LambdaP/(h*c*AeffP)) ;
signalinfo = (LambdaS*GammaS/(h*c*AeffS )); %2.7
```

```
%980 pump absorptions
RESA = N2(j,i)*sigma26*pumpinfo980*(PumpForw(i) + PumpBack(i))*GammaP;
RGSA= NO(j,i)*sigma02*pumpinfo980*(PumpForw(i) + PumpBack(i))*GammaP;
% Possible Stimulated Emission
%
      SE10(j+1,i) = (b1*N1(i)-(g1/g2)*b0*N0(i))*sigma15*c*Phi21(j,i); % 1.5 um
%
      SE20(j+1,i) = (b2*N2(i)-(g2/g1)*b1*N0(i))*sigma21*c*Phi20(j,i); % 980 nm
%
      SE51(j+1,i) = (b2*N2(i)-(g5/g1)*b1*N1(i))*sigma15*c*Phi51(j,i); % 850 nm
%
      SE50(j+1,i) = (b2*N2(i)-(g5/g0)*b0*N0(i))*sigma15*c*Phi50(j,i); % 550 nm
RSE21 = (b2*N2(j,i)-(g2/g1)*b1*N1(j,i))*sigma21*(signalForw(i)+signalBa...
ck(i)); % LASING AT 2.7 um
k1N6 = (-N6(j,i)/t6 + W22*N2(j,i).^2 + RESA);
k1N5 = (-N5(j,i)/t5 - W50*N5(j,i).*N0(j,i) + B65*N6(j,i)/t6);
k1N4 = (-N4(j,i)/t4 + B54*1/t5*N5(j,i));
k1N3 = (-N3(j,i)/t3 + B43*1/t4*N4(j,i) + W50*N5(j,i).*N0(j,i) + W11.*N1...
(j,i).^2 + B53*1/t5*N5(j,i));
k1N2 = (-N2(j,i)/t2 + B32*1/t3*N3(j,i) + RGSA - RESA - RSE21*signalinfo...
-2*W22.*N2(j,i).^2 + B52*1/t5*N5(j,i));
k1N1 = (-N1(j,i)/t1 + B21*1/t2*N2(j,i) + B51*1/t5*N5(j,i) + RSE21*...
signalinfo + W50.*N5(j,i).*N0(j,i) - 2*W11.*N1(j,i).^2);
k2N6 = N6(j,i) + dt/2* k1N6;
k2N5 = N5(j,i) + dt/2* k1N5;
k2N4 = N4(j,i) + dt/2* k1N4;
k2N3 = N3(j,i) + dt/2* k1N3;
k2N2 = N2(j,i) + dt/2* k1N2;
k2N1 = N1(j,i) + dt/2* k1N1;
```

```
k3N6 = N6(j,i) + dt/2* k2N6;
k3N5 = N5(j,i) + dt/2* k2N5;
k3N4 = N4(j,i) + dt/2* k2N4;
k3N3 = N3(j,i) + dt/2* k2N3;
k3N2 = N2(j,i) + dt/2* k2N2;
k3N1 = N1(j,i) + dt/2* k2N1;
k4N6 = N6(j,i) + dt* k3N6;
k4N5 = N5(j,i) + dt* k3N5;
k4N4 = N4(j,i) + dt* k3N4;
k4N3 = N3(j,i) + dt* k3N3;
k4N2 = N2(j,i) + dt* k3N2;
k4N1 = N1(j,i) + dt* k3N1;
N6(j+1,i) = N6(j,i) + dt/6*(k1N6 + 2*k2N6 + 2*k3N6 + k4N6);
N5(j+1,i) = N5(j,i) + dt/6*(k1N5 + 2*k2N5 + 2*k3N5 + k4N5);
N4(j+1,i) = N4(j,i) + dt/6*(k1N4 + 2*k2N4 + 2*k3N4 + k4N4);
N3(j+1,i) = N3(j,i) + dt/6*(k1N3 + 2*k2N3 + 2*k3N3 + k4N3);
N2(j+1,i) = N2(j,i) + dt/6*(k1N2 + 2*k2N2 + 2*k3N2 + k4N2);
N1(j+1,i) = N1(j,i) + dt/6*(k1N1 + 2*k2N1 + 2*k3N1 + k4N1);
NO(j+1,i) = Nt - N1(j,i) - N2(j,i) - N3(j,i) - N4(j,i) - N5(j,i) - N6(j,i);
if((j<1000))
% [N1(j,1),N2(j,1),N3(j,1),N4(j,1),N5(j,1),j]
```

```
end
if (Nt < N2(j,i))
break
end
end
%
% Pp(i+1) = Pp(i)*exp(-(sigma03*NO(j,i)+sigma15*N1(j,i)+sigma27*N2(j,i))*dz);
%
%
% Phi21(1,i+1) = Phi21(Tsub,i);
SpontEM2700 = N2(Tsub,i)*B21*rcore^2*pi*(2700e-9)^-1*(h*c)/t2*.318;
% SpontEM1500 = .63*N1(Tsub,i)*B10*rcore^2*pi*(1500e-9)^-1*(h*c)/t1*1e-1;
% SpontEM980 = .63*N2(Tsub,i)*B20*rcore^2*pi*(980e-9)^-1*(h*c)/t2*.3e-1;
% SpontEM850 = .63*N5(Tsub,i)*B51*rcore^2*pi*(850e-9)^-1*(h*c)/t5*.3e-1;
% SpontEM1700 = .63*N1(Tsub,i)*B10*rcore^2*pi*(1500e-9)^-1*(h*c)/t1*.3e-1;
% SpontEM550 = .63*N5(Tsub,i)*B50*rcore^2*pi*(550e-9)^-1*(h*c)/t5;
alpha(i) = sigma02*N0(Tsub,i)+sigma26*N2(Tsub,i);
if mod(Q,2)==1
Pp980(i+1) = Pp980(i)*exp(-alpha(i)*dz);
PumpForw(i+1) = PumpForw(i) - dz*(alpha(i)*PumpForw(i)*GammaP + 3e-3*PumpForw(i));
signalForw(i+1) = (signalForw(i) + dz*(.01*SpontEM2700+ (b2*N2(j,i)-(g2/g1)...
*b1*N1(j,i))*sigma21*GammaS*signalForw(i) -23e-3*signalForw(i)));
```

```
else
% Pp980(i) = Pp980(i)*exp(-alpha(i)*dz);
PumpBack(i+1) = PumpBack(i) - dz*(alpha(i)*PumpBack(i)*GammaP + 3e-3*PumpBack(i));
signalBack(i+1) = (signalBack(i) + dz*(.01*SpontEM2700+ (b2*N2(j,i)-...
(g2/g1)*b1*N1(j,i))*sigma21*GammaS*signalBack(i) -23e-3*signalBack(i));
end
end
OutPut(Q) = (1-Rs2)*signalForw(Nsub-1);
if Q>1 && mod(Q,2)==1 && (abs(OutPut(Q) - OutPut(Q-2))/(OutPut(Q))<0.01)
Q
(OutPut(Q) - OutPut(Q-2))/(OutPut(Q))
break
end
if Q ~= RoundTrips
if mod(Q,2) == 1
signalBack(1) = (Rs2)*signalForw(Nsub);
PumpBack(1) = (Rp2)*PumpForw(Nsub);
PumpForw = PumpForw(end:-1:1);
signalForw = signalForw(end:-1:1);
else
```

```
signalForw(1) = (Rs1)*signalBack(Nsub);
PumpForw(1) = (Rp1)*PumpBack(Nsub)+Ppo980;
PumpBack = PumpBack(end:-1:1);
signalBack = signalBack(end:-1:1);
end
else
Signalout = (1-Rs2)*signalForw(Nsub)
end
end
figure,
subplot(3,1,1)
plot(t,N0(:,1),'k-',t,N2(:,1),'b-', t,N1(:,1),'g-',t,N5(:,1),'m-')
legend('NO ', 'N2 ', 'N1','N5')
title('Population Levels at Beginning of Fiber')
xlabel('Time(s)')
ylabel('pop. density Ions/m^3')
subplot(3,1,2)
plot(t,N2(:,Nsub/2),'b-', t,N1(:,Nsub/2),'g-',t,N5(:,Nsub/2),'m-')
legend( 'N2 ', 'N1', 'N5')
title('Population Levels @ Middle of Fiber')
xlabel('Time(s)')
```

```
ylabel('Pop. density (Ions/m<sup>3</sup>)')
subplot(3,1,3)
plot(t,N2(:,Nsub),'b-', t,N1(:,Nsub),'g-',t,N5(:,Nsub),'m-')
legend('N2 ', 'N1','N5')
title('Population Levels @ End of Fiber')
xlabel('Time(s)')
ylabel('Pop. density (Ions/m^3)')
figure,
subplot(2,1,1)
plot(z,signalForw,'m-')
legend('Signal')
title('Signal power vs distance')
xlabel(' Distance (m)')
ylabel('Signal power (W)')
subplot(2,1,2)
plot(z,PumpForw,'m')
title('Pump power vs distance')
xlabel('Distance along fiber (m)
ylabel('Pump Power (W)')
```

% omega = 500:10:3000;

```
% siz0 = length(omega);
% dOmeg = 1/10;
% Spectrum = zeros(1,siz0);
% Spectrum(round((850-500)*d0meg)+1)= Signal51(end);
% Spectrum(round((550-500)*d0meg)+1)= Signal50(end);
% Spectrum(round((1500-500)*d0meg)+1)= Signal10(end);
% % Spectrum(round((980-500)*d0meg)+1)= Signal20(end);
% Spectrum(round((1700-500)*d0meg)+1)= Signal53(end);
% Spectrum(round((2700-500)*d0meg)+1)= Signal(end);
% Spectrum(round((980-500)*d0meg)+1)= Pp980(end)+Signal20(end);
% figure,
% plot(omega,Spectrum,'k-')
% [1] M. Pollnau, S. Bedo, w. Luthy, H.P and Weber, 'On the saturation of
%the 791 nm pumped erbium 3 um fiber laser.'' Tech. Dig. Conf. Advanced Solid-State L
%[2] M. Pollnau, Ch. Ghisler, G. Bunea, M. Bunea, W. Lthy, and H.P. Weber,
%''150 mW unsaturated output power at 3 $\mu$m from a single-mode-fiber erbium cascad
%[3] M. Pollnau and S. D. Jackson, ''Energy recycling versus lifetime quenching
%in erbium-doped 3-$\mu$m fiber lasers,'' IEEE Journal of Quantum Electronics, vol. 3
```